

Analytical Modeling of Impact Resistance and Damage Tolerance of Laminated Cylindrical Shells

K.Y. Huang *

Crea Mech Company, Ltd., 201203 Shanghai, People's Republic of China

This paper is devoted to an analytical model for the prediction of impact resistance and damage tolerance properties of cylindrical composite shells by pursuing the energetic approach. At the most fundamental level, the existing theories of thin elastic shells are unified with each other. The snap-through buckling problem is subsequently solved through a large deflection analysis. After that, the impact induced damage development process is analyzed by using the fracture and damage mechanics concepts that form a synergetic combination. For the residual compression strength, a new theory is proposed, where the emphasis is placed on the identification of the lowest buckling mode and the derivation of a complete postbuckling solution. The model is verified by a series of curved panel impact and compression-after-impact experiments, and a good agreement is found to exist between the theoretical and experimental results.

*General Manager, Guoshoujing Road 351.

Nomenclature

a	Shell length or major semi-axis of ellipse
A	Extensional stiffness or crack area
b	Curved shell width or minor semi-axis of ellipse
D	Bending stiffness
E	Elastic modulus or impact energy
G	Energy release rate
h	Shell thickness
K	Membrane stiffness or curvature parameter
l	Characteristic shell length
M	Bending moment per length unit
N	Normal force per length unit
P	Impact load
q	Distributed load
R	Shell radius
S	Area of damage zone
u	In-plane displacement
U	Strain energy
v	In-plane displacement
w	Out-of-plane displacement
γ	Shear strain
δ	Deflection
ϵ	Normal strain
ζ	Energy reduction factor
θ	Orientation angle of delamination
κ	Change in curvature
λ	Ellipticity ratio
Λ	Objective function for minimization
ν	Poisson's ratio
σ	Normal stress
τ	Shear stress
ϕ	Airy stress function
Ψ	Membrane stiffness parameter

I. Introduction

With fiber reinforced composite materials being increasingly used in primary aircraft structures, accurate prediction methods for impact resistance and damage tolerance properties of composite structures become more and more important for an effective and efficient design process. The closed form analytical solutions are evidently of great fundamental and practical interest; as they not only provide a clear understanding of the underlying physics, but also reduce the computational expense tremendously in comparison with finite element calculations. By means of the plate theory, linear elastic fracture mechanics (LEFM) and theory of elastic stability, an analytical model has been formulated for flat plates subjected to low velocity impact and post-impact compression in the previous study (see Huang et al.¹). Compared with the experimental results, the model appears to be capable of giving realistic predictions of the delamination threshold load, the resulting damage area and the residual compression strength for different flat plates.

There now arises the question whether the flat plate model is directly applicable to cylindrical shells, as thin-walled shell structures are more frequently encountered in the aerospace applications, for example in the fuselages and wings (see Raymer²). Ambur and Starnes³ conducted impact and compression-after-impact (CAI) tests on thin quasi-isotropic cylindrical graphite-epoxy shells, it was found that the peak contact force and the CAI residual strength are curvature dependent. Wardle and Lagace⁴ performed quasi-static and impact tests on cylindrical graphite-epoxy shells, they came to the conclusion that the extent of damage is dependent of the peak contact load and the snap-through buckling phenomenon during the impact events significantly affects the damage development. These experimental findings suggest that the flat plate model, which is valid for the special limiting case of shells having no curvature, will not be appropriate for general cylindrical shells. This provides the motivation to build upon and extend the previous model, whilst still retaining the essential simplicity of the original. The objective of the present study is to develop a reliable and robust analytical model for the impact resistance and damage tolerance characteristics of thin cylindrical shells by adopting the energetic approach. It can be expected that a number of difficult and long-standing problems have to be solved to accomplish the intended model.

The first challenge faced in this study is the unification of theories for thin elastic shells. On the basis of different simplifying assumptions, different investigators have developed different shell theories (see Flügge⁵, Koiter⁶ and Sanders⁷, Love⁸, Morley⁹, Simmonds¹⁰, Donnell¹¹, Lord Rayleigh¹²). For a comprehensive review of the existing shell theories, the reader is referred to Leissa¹³. The essence of the shell theories is that a complex three-dimensional elasticity problem is consistently reduced to a workable two-dimensional problem by using the Kirchhoff hypotheses¹⁴ that proved successful for flat plates. Among the investigators

in this field, it has been a subject of considerable discussions about the consistent treatment of small terms in a purely mathematical sense, i.e. which terms can be retained and which can be neglected, or whether they are of the same order. Since the complexity of a shell theory depends strongly on the behavior of the infinitesimal shell elements, one has to take a new perspective and start to think over whether the infinitesimal elements that are basically points from a geometrical standpoint should have a curved or squared shape.

The second challenge is to come to a full understanding of the large deflection behavior of cylindrical shells. It is still unclear what precisely happens, when a cylindrical shell undergoes the snap-through buckling. This kind of problem is usually solved through sophisticated numerical simulations, where the arc-length method is employed, as the powerful Newton-Raphson method becomes unstable in the neighborhood of the limit point (see Riks¹⁵). Using the Galerkin method, an analytical solution has been derived for the snap-through buckling of a uniformly compressed cylindrical shell that behaves like a circular arch (see Ventsel and Krauthammer¹⁶). This gives a valuable clue that the snap-through buckling problem must be analytically solvable for more complex cases.

The third challenge is a large-scale reformation of the buckling and postbuckling theory of cylindrical shells. As is known, the Lorenz¹⁷ theory overestimates the actual buckling strength to a large extent. This has led to the development of theories which believe that the initial imperfections are the most influential contributor to the discrepancy between the predictions and measurements (see Timoshenko & Gere¹⁸). A linearized buckling theory is only in a position to predict the first equilibrium path up to the bifurcation point. The initial postbuckling theory of Koiter¹⁹ is a higher order linearization that permits determination of the slopes and the curvature of the second equilibrium path at the bifurcation point. As the name implies, for general cylindrical shells, the theory is not valid for the second equilibrium path well in excess of the initial buckling load. Furthermore, it would be a laborious task to extend this complicated theory to an anisotropic version. This necessitates the construction of a simpler and deeper theory for the buckling and postbuckling behavior of cylindrical shells.

II. Fundamentals

The two cornerstones of a shell theory are the elasticity theory and the differential geometry. The elasticity theory delivers the three sets of fundamental equations concerning the static equilibrium, the constitutive behavior and the compatibility conditions. Using the differential geometry, the strain displacement relations can be derived in a rigorous way. The equations obtained are solved for the given boundary conditions, where both the mathematical techniques and the mechanical intuition are indispensable.

A. Brief Outline of Shell Theories

Among the aforementioned shell theories, Love's theory is a general and elegant theory, with which the stress, strain, and displacement fields can be adequately predicted under the small deflection condition. For anisotropic shells, Love's theory can be used in conjunction with the classical lamination theory (CLT), which characterizes the constitutive behavior of a laminate with the familiar ABD matrix by way of the Kirchhoff-Love hypotheses (see Jones²⁰). Compared with Flügge's theory, the infinitesimal elements are essentially flat in Love's theory; therefore, the curvature related couplings between the extension, shear, bending and twist deformations are neglected on the scale of the infinitesimal elements. Compared with Koiter-Sanders theory, the rotation of the infinitesimal elements around the normal is neglected in Love's theory. For cylindrical shells, Morley's theory is derived from Flügge's theory, and Simmonds' theory is derived from Koiter-Sanders theory. These simplified theories give practically the same predictions as the original theories, but a clear physical meaning has not been assigned to the higher order terms neglected. If it can be substantiated that the theories of Love, Morley and Simmonds are equivalent to each other for cylindrical shells, it can be established that the geometrical coupling effects and the rotational effects in the infinitesimal elements are secondary effects in relation to the primary effects due to stretching and bending. In this way, the different shell theories can be unified with each other. When the wavelength of the deformation pattern is sufficiently small, Donnell's theory, which can be deduced from Love's theory by neglecting the influence of the in-plane displacements on the curvature changes, represents the simplest valid form. Lord Rayleigh's inextensional deformation theory applies to the special cases in which the shell deformations consist primarily in bending. For a large deflection analysis, the geometrical non-linearity in the membrane deformations can be taken into account by using von Kármán strains²¹ that can be viewed as sort of simplified Green-Lagrange strains. It can still be assumed that the curvature changes are linear functions of the displacements, as the membrane and bending deformations are related to the first and second fundamental form of the shell middle surface, respectively. The shell theories are a two-dimensional analogue of the one-dimensional Euler-Bernoulli beam theory, and are therefore not applicable to the open shells that undergo significant warping owing to torsion. For the rest, the theories incorporating the transverse shear and normal stress effects and the specialized theories for shells of revolution are left out of consideration in this study.

B. Membrane Problem

Consider a doubly curved composite shell, the principal radii of curvature are R_1 and R_2 , the orthogonal curvilinear coordinates x and y follow the lines of curvature, and the positive z direction coincides with the inward direction. For the constitutive behavior of the laminate, the following equation is valid in accordance

with the CLT:

$$\begin{Bmatrix} N \\ M \end{Bmatrix} = \begin{bmatrix} A & B \\ B & D \end{bmatrix} \begin{Bmatrix} \epsilon \\ \kappa \end{Bmatrix} \quad (1)$$

where $\{N\}$, $\{M\}$, $\{\epsilon\}$ and $\{\kappa\}$ are the vectors of resultant membrane forces, resultant bending moments, membrane strains and curvature changes, respectively; $[A]$, $[B]$ and $[D]$ are the extensional stiffness matrix, the bending-extension matrix and the bending stiffness matrix, respectively. In light of practical structural applications, the laminate is supposed to have a symmetrical and balanced lay-up. This means that the bending-extension coupling does not occur, nor does the shear-extension coupling occur, i.e. $A_{16} = A_{26} = 0$, $[B] = [0]$. When the laminate is fabricated solely of 0° and 90° laminae, the bend-twist coupling does not occur, i.e. $D_{16} = D_{26} = 0$. If the laminate has off-axis plies, the bend-twist coupling can be diminished by increasing the number of ply groups. For the in-plane equilibrium, an Airy stress function ϕ can be introduced for the resultant membrane forces N_x , N_y and N_{xy} :

$$N_x = \frac{\partial^2 \phi}{\partial y^2}, \quad N_y = \frac{\partial^2 \phi}{\partial x^2}, \quad N_{xy} = -\frac{\partial^2 \phi}{\partial x \partial y} \quad (2)$$

Adding the non-linear terms to Love's strain displacement relations, the following equations can be set up:

$$\epsilon_x = \frac{\partial u}{\partial x} - \frac{w}{R_1} + \frac{1}{2} \left(\frac{\partial w}{\partial x} \right)^2 = S_{11} \frac{\partial^2 \phi}{\partial y^2} + S_{12} \frac{\partial^2 \phi}{\partial x^2} \quad (3)$$

$$\epsilon_y = \frac{\partial v}{\partial y} - \frac{w}{R_2} + \frac{1}{2} \left(\frac{\partial w}{\partial y} \right)^2 = S_{12} \frac{\partial^2 \phi}{\partial y^2} + S_{22} \frac{\partial^2 \phi}{\partial x^2} \quad (4)$$

$$\gamma_{xy} = \frac{\partial v}{\partial x} + \frac{\partial u}{\partial y} + \frac{\partial w}{\partial x} \frac{\partial w}{\partial y} = -S_{66} \frac{\partial^2 \phi}{\partial x \partial y} \quad (5)$$

where u and v are the in-plane displacements, w is the out-of-plane displacement, and $[S]$ is the compliance matrix with $[S] = [A]^{-1}$. Eliminating u and v yields the biharmonic equation for the plane stress problem:

$$\nabla_S^4 \phi = \left(\frac{\partial^2 w}{\partial x \partial y} \right)^2 - \frac{\partial^2 w}{\partial x^2} \frac{\partial^2 w}{\partial y^2} - \frac{1}{R_2} \frac{\partial^2 w}{\partial x^2} - \frac{1}{R_1} \frac{\partial^2 w}{\partial y^2} \quad (6)$$

where the differential operator ∇_S^4 is defined as:

$$\nabla_S^4(\cdot) = S_{22} \frac{\partial^4}{\partial x^4} + 2J \frac{\partial^4}{\partial x^2 \partial y^2} + S_{11} \frac{\partial^4}{\partial y^4} \quad \text{with} \quad J = S_{12} + \frac{S_{66}}{2} \quad (7)$$

In this way, a set of equations concerning the equilibrium, constitutive and compatibility of the shell is reduced to one single equation. The homogenous solution of differential equation (6) describes the characteristic in-plane behavior of the system, e.g. from $\nabla_S^4 \phi = 0$, the distribution of the membrane stresses around a hole

in a laminate can be solved. The particular solution represents the forced response of the system to the out-of-plane displacement field w . In spite of the fact that the geometrical couplings are neglected on the scale of the infinitesimal elements, the in-plane and out-of-plane displacements are generally coupled to each other on the global structural scale because of the geometrical non-linearity and the initial curvature.

C. Bending Problem

The counterpart of the membrane problem, the bending problem, is discussed on the basis of a cylindrical shell, since the equations can be readily extended to a doubly curved shell. For the moment equilibrium of an infinitesimal shell element, the following equation can be set up:

$$\frac{\partial^2 M_x}{\partial x^2} + 2\frac{\partial^2 M_{xy}}{\partial x \partial y} + \frac{\partial^2 M_y}{\partial y^2} - \frac{N_y}{R} = q \quad (8)$$

where R is the shell radius and q is the transverse load. According to Love, the equations for the curvature changes that strictly conform to the differential geometry are as follows:

$$\kappa_x = \frac{\partial^2 w}{\partial x^2}, \quad \kappa_y = \frac{1}{R} \frac{\partial v}{\partial y} + \frac{\partial^2 w}{\partial y^2}, \quad \kappa_{xy} = \frac{1}{R} \frac{\partial v}{\partial x} + 2\frac{\partial^2 w}{\partial x \partial y} \quad (9)$$

In Lord Rayleigh's theory, the expression of κ_{xy} does not contain the factor 2, as the term $\frac{\partial^2 w}{\partial y \partial x}$ was not allowed for during the derivation. Using equations (1) and (9), the bending equation (8) can be rewritten in the form of a biharmonic equation:

$$\nabla_D^4 w + \frac{1}{R} \nabla_d^2 \left(\frac{\partial v}{\partial y} \right) = q + \frac{1}{R} \frac{\partial^2 \phi}{\partial x^2} \quad (10)$$

where the bend-twist coupling is neglected to facilitate the analysis, and the differential operators ∇_D^4 , ∇_d^2 and the constant H are defined as:

$$\nabla_D^4(\cdot) = D_{11} \frac{\partial^4}{\partial x^4} + 2H \frac{\partial^4}{\partial x^2 \partial y^2} + D_{22} \frac{\partial^4}{\partial y^4}, \quad \nabla_d^2(\cdot) = H \frac{\partial^2}{\partial x^2} + D_{22} \frac{\partial^2}{\partial y^2}, \quad H = D_{12} + 2D_{66} \quad (11)$$

Neglecting the influence of the circumferential strain ϵ_y on the curvature changes with $\partial v / \partial y \approx w / R$, equation (10) can be simplified to:

$$\nabla_D^4 w + \frac{1}{R^2} \nabla_d^2 w = q + \frac{1}{R} \frac{\partial^2 \phi}{\partial x^2} \quad (12)$$

Setting $R \rightarrow \infty$, it can be seen that the biharmonic part is associated with the transverse loading q . The Laplacian part can be linked up with the distributed moment produced by the circumferential membrane

stress N_y , where the out-of-plane displacement w exhibits typically a very slow decay behavior. Although the membrane and bending problem can be mathematically formulated as two separate problems, the two problems are coupled to each other because of the coexistence of the membrane and bending deformations.

D. Equivalency of Theories

To provide a simple proof, the equivalency validation is restricted to the small deflection analysis of an isotropic cylindrical shell, as the differences between the theories are known to exist mainly in the bending problem. Discarding the non-linear terms, the biharmonic membrane equation (6) becomes:

$$\nabla^4 \phi = -\frac{Eh}{R} \frac{\partial^2 w}{\partial x^2} \quad (13)$$

where E is the Young's modulus. Combined with the Laplace equation $\nabla^2 \phi = 0$ that means a state of zero hydrostatic deformation (no volume change), equation (13) can be put in the following form:

$$\nabla^4 \phi + \frac{1}{R^2} \nabla^2 \phi = -\frac{Eh}{R} \frac{\partial^2 w}{\partial x^2} \quad (14)$$

On the basis of the isotropy, the biharmonic bending equation (12) can be simplified to:

$$\nabla^4 w + \frac{1}{R^2} \nabla^2 w = \frac{q}{D} + \frac{1}{RD} \frac{\partial^2 \phi}{\partial x^2} \quad (15)$$

where D is the flexural rigidity. It can be observed that equations (14) and (15) are identical to Simmonds' equation using a complex-valued displacement-stress function.

Substituting equation (13) into equation (15), the following eighth order differential equation can be obtained, showing that the applied load is carried through a combination of bending and stretching actions:

$$\nabla^4 (\nabla^4 + R^{-2} \nabla^2) w + 4C^4 \frac{\partial^4 w}{\partial x^4} = \frac{1}{D} \nabla^4 q, \quad 4C^4 = \frac{12(1-\nu^2)}{R^2 h^2} \quad (16)$$

where ν is the Poisson's ratio, h is the shell thickness. Adding $R^{-2} \nabla^2 (\nabla^4 + R^{-2} \nabla^2) w = 0$ to equation (16) yields Morley's equation:

$$\nabla^4 (\nabla^2 + R^{-2})^2 w + 4C^4 \frac{\partial^4 w}{\partial x^4} = \frac{1}{D} \nabla^4 q \quad (17)$$

From equation (15), it can be seen that the homogenous equation $(\nabla^4 + R^{-2} \nabla^2) w = 0$ describes actually the deflection behavior of the shell in the absence of the transverse loading and the circumferential stretching. A practical example is the deflection produced by a moment along the edge, which can be specified through the boundary condition in equation (16).

Taken together, it has been demonstrated that the theories of Love, Morley and Simmonds are equivalent to each other. It is clear that Love's theory truly deserves the designation of the classical shell theory, as the mathematical exactness is perfectly balanced with the responsible simplifications in this theory. The more complex theories of Flügge, Koiter and Sanders are more favorable for finite element analyses, where the effects of geometrically couplings and rotations about the normal have to be taken into account in the discrete elements.

E. Donnell's Simplified Theory

By neglecting the terms $\partial v/\partial x$ and $\partial v/\partial y$, Donnell's expressions for the curvature changes become similar to those in the plate theory:

$$\kappa_x = \frac{\partial^2 w}{\partial x^2}, \quad \kappa_y = \frac{\partial^2 w}{\partial y^2}, \quad \kappa_{xy} = 2 \frac{\partial^2 w}{\partial x \partial y} \quad (18)$$

For the linear analysis of an anisotropic cylindrical shell, the biharmonic equations (6) and (12) reduce to:

$$\nabla_S^4 \phi = -\frac{1}{R} \frac{\partial^2 w}{\partial x^2}, \quad \nabla_D^4 w = q + \frac{1}{R} \frac{\partial^2 \phi}{\partial x^2} \quad (19)$$

Combining the equations above with each other, the generalized equation of Donnell can be written as:

$$\nabla_S^4 \nabla_D^4 w + \frac{1}{R^2} \frac{\partial^4 w}{\partial x^4} = \nabla_S^4 q \quad (20)$$

In the isotropic case, Donnell's equation reads:

$$\nabla^8 w + 4C^4 \frac{\partial^4 w}{\partial x^4} = \frac{1}{D} \nabla^4 q \quad (21)$$

Introducing the non-dimensional parameters:

$$\varrho = \frac{x}{R}, \quad \varphi = \frac{y}{R}, \quad 4c^4 = 12(1 - \nu^2) \frac{R^2}{h^2} \quad (22)$$

and taking an eigenfunction in the form:

$$w = e^{p\varrho} \cos n\varphi \quad (23)$$

the characteristic equations of Donnell's equation (21) and Morley's equation (17) become:

$$\begin{aligned} \text{Donnell : } & (p^2 - n^2)^4 + 4c^4 p^4 = 0 \\ \text{Morley : } & (p^2 - n^2)^2 (p^2 - n^2 + 1)^2 + 4c^4 p^4 = 0 \end{aligned} \quad (24)$$

If $n \geq 4$, then 1 can be neglected in relation to n^2 , Morley's equation that covers the complete range of wavelengths reduces to Donnell's equation; and if $n \gg \sqrt{2/3}c^2$, then the term $4c^4p^4$ can be neglected, Donnell's equation reduces further to the flat plate equation in the cylindrical coordinates (see Figure 1). In Lord Rayleigh's theory, the term 1 is unnecessarily retained, as it hardly affects the outcome when the term $4c^4p^4$ can be neglected. For an extremely small thickness h , the term $\nabla^8 w$ can be neglected, and Donnell's equation reduces to a membrane equation. It can be construed that Donnell's theory is sufficiently accurate for technical applications, as long as the wavelength of the deformation pattern does not exceed a quarter of the shell circumference. For a symmetrically loaded full cylindrical shell ($n = 0$), Donnell's theory is exact, since there holds $v = 0$. The frequently used name in the literature, "the shallow shell approximation", might be said to be imprecise. Despite the restricted applicability, Donnell's theory, the engineering shell theory, has reached the stage of ultimate simplicity.

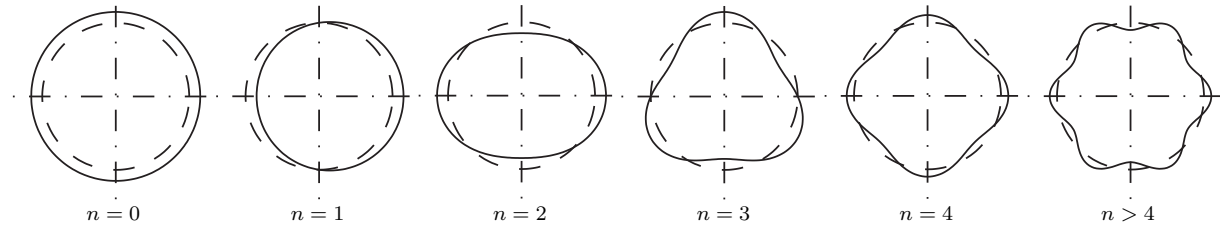


Figure 1. Eigenfunction $w = e^{p\varrho} \cos n\varphi$ with varying n for $\varrho = 0$

F. Energy Functional

For a laminated shell having a symmetrical and balanced lay-up, the total strain energy is given by:

$$\begin{aligned}
 U = & \frac{1}{2} \iint_S (S_{11}N_x^2 + 2S_{12}N_xN_y + S_{22}N_y^2 + S_{66}N_{xy}^2) dx dy \\
 & + \frac{1}{2} \iint_S (D_{11}\kappa_x^2 + 2D_{12}\kappa_x\kappa_y + D_{22}\kappa_y^2 + D_{66}\kappa_{xy}^2) dx dy \\
 & + \frac{1}{2} \iint_S (2D_{16}\kappa_x\kappa_{xy} + 2D_{26}\kappa_y\kappa_{xy}) dx dy
 \end{aligned} \tag{25}$$

For the membrane energy, the forces N_x , N_y and N_{xy} can be calculated from the stress function ϕ using equation (2). For the bending energy, the curvature changes κ_x , κ_y and κ_{xy} can be calculated from the displacements u , v and w using the following formulas of Love:

$$\kappa_x = \frac{1}{R_1} \frac{\partial u}{\partial x} + \frac{\partial^2 w}{\partial x^2}, \quad \kappa_y = \frac{1}{R_2} \frac{\partial v}{\partial y} + \frac{\partial^2 w}{\partial y^2}, \quad \kappa_{xy} = \frac{1}{R_1} \frac{\partial u}{\partial y} + \frac{1}{R_2} \frac{\partial v}{\partial x} + 2 \frac{\partial^2 w}{\partial x \partial y} \tag{26}$$

If the out-of-plane displacement field w is symmetrical with respect to the x and y axes, it is expected that the D_{16} and D_{26} terms vanish in equation (25), as the displacement field does not contain the asymmetrical

bending deformation components that arise out of the bend-twist coupling. The energy functional (25) that contains the full information of the three sets of the elasticity equations is of use for many purposes: The shell deflection problems can be dealt with by means of the principle of virtual work. The shell buckling problems can be solved through the principle of critical energy, which states that buckling occurs, when the work performed by the membrane forces due to the lateral deflections equals or exceeds the total strain energy that is associated with the lateral deflections. The shell vibration problems can be formulated on the basis of Hamilton's principle; however, this topic lies beyond the scope of this study.

III. Localized Snap-through Buckling

Before describing the main body of the impact resistance and damage tolerance analysis, it is useful to discuss the snap-through buckling problem, particularly the reversal of curvature of the shell surface in an elliptic domain that is sufficiently remote from the shell edges. This form of localized snap-through buckling is a basic deformation mechanism in thin elastic shells. Hence, the analytical solution obtained is expected to find many applications in structural analyses. For the impact modeling, the solution plays an important role in the determination of the energy release rate that drives the crack extension. For a complete cylindrical shell under axial compression, the solution provides a "Rosetta stone" for understanding the buckling process.

A. Membrane and Bending Energy

Consider a doubly curved shell in the curvilinear coordinates x and y , the principal radii of curvature are R_1 and R_2 . The elliptic region that has curved semi-axes a_0 and b_0 is subjected to a uniformly distributed load q . It is supposed that the elliptic shell segment is simply supported in the out-of-plane directions by the surrounding shell (see Figure 2).

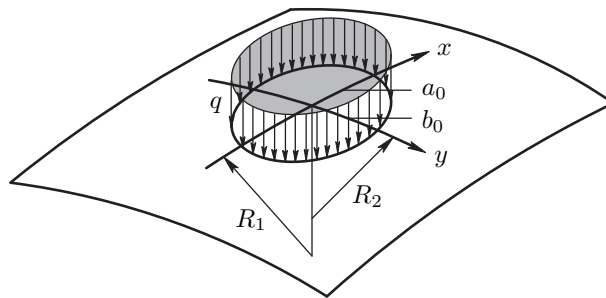


Figure 2. Uniformly loaded elliptic domain

Substituting the following displacement field w into the biharmonic membrane equation (6):

$$w = w_0 \left(1 - \frac{x^2}{a_0^2} - \frac{y^2}{b_0^2} \right) \quad (27)$$

gives a biharmonic equation with a constant right-hand side:

$$\nabla_S^4 \phi = \frac{2w_0}{a_0^2 b_0^2} \left(\frac{a_0^2}{R_1} + \frac{b_0^2}{R_2} - 2w_0 \right) \quad (28)$$

The function w stems from an elliptic isotropic plate that is simply supported along the edge and uniformly loaded in the lateral direction (see Timoshenko and Woinowsky-Krieger²²). A suitable expression for the Airy stress function that satisfies the simply supported boundary condition is:

$$\phi = \frac{w_0}{4\Upsilon} \left(\frac{a_0^2}{R_1} + \frac{b_0^2}{R_2} - 2w_0 \right) \left(1 - \frac{x^2}{a_0^2} - \frac{y^2}{b_0^2} \right)^2 \quad (29)$$

where the parameter Υ and the ellipticity ratio λ_0 are given by:

$$\Upsilon = 3\lambda_0^2 S_{22} + 2J + 3\lambda_0^{-2} S_{11}, \quad \lambda_0 = \frac{b_0}{a_0} \quad (30)$$

Integrating over the elliptic domain, the membrane energy U_m becomes:

$$U_m = \frac{\pi^2 w_0^2}{12S\Upsilon} \left(\frac{a_0^2}{R_1} + \frac{b_0^2}{R_2} - 2w_0 \right)^2 \quad (31)$$

where S is the area of the elliptic shell segment, $S = \pi a_0 b_0$.

Employing the simplifications $\partial u/\partial x \approx w/R_1$ and $\partial v/\partial y \approx w/R_2$, the curvature change expressions from Love's theory can be rewritten as:

$$\kappa_x = \frac{w}{R_1^2} + \frac{\partial^2 w}{\partial x^2}, \quad \kappa_y = \frac{w}{R_2^2} + \frac{\partial^2 w}{\partial y^2}, \quad \kappa_{xy} = \frac{1}{R_1^2} \frac{\partial}{\partial y} \int w dx + \frac{1}{R_2^2} \frac{\partial}{\partial x} \int w dy + 2 \frac{\partial^2 w}{\partial x \partial y} \quad (32)$$

Neglecting the higher order terms containing R_1^{-4} , $R_1^{-2}R_2^{-2}$ and R_2^{-4} , the bending energy U_b is found to be:

$$U_b = \frac{2\pi^2 (\Phi - \Phi') w_0^2}{S} \quad (33)$$

where the parameters Φ and Φ' are given by:

$$\Phi = \lambda_0^2 D_{11} + 2D_{12} + \lambda_0^{-2} D_{22} \quad (34)$$

$$\Phi' = \frac{a_0 b_0}{2} \left[\frac{\lambda_0}{R_1^2} D_{11} + \left(\frac{\lambda_0^{-1}}{R_1^2} + \frac{\lambda_0}{R_2^2} \right) D_{12} + \frac{\lambda_0^{-1}}{R_2^2} D_{22} \right] \quad (35)$$

Hence, the total strain energy U becomes:

$$U = \frac{\pi^2 w_0^2}{12S\Upsilon} \left(\frac{a_0^2}{R_1} + \frac{b_0^2}{R_2} - 2w_0 \right)^2 + \frac{2\pi^2(\Phi - \Phi')w_0^2}{S} \quad (36)$$

If it can be assumed that $R_1 \gg a_0$ and $R_2 \gg b_0$, then Donnell's theory can be applied instead of Love's theory, and the parameter Φ' becomes automatically equal to 0.

B. Load Deflection Relationship

The relationship between the distributed load q and the maximum deflection w_0 can be derived on the basis of the principle of virtual displacements:

$$\frac{dU}{dw_0} \delta w_0 = \iint_S q \delta w_0 \left(1 - \frac{x^2}{a_0^2} - \frac{y^2}{b_0^2} \right) dx dy \quad (37)$$

From equation (37), it follows that:

$$\frac{3\Upsilon S^2 q}{\pi^2 h^3} = 8 \frac{w_0^3}{h^3} - 6 \left(\frac{a_0^2}{R_1 h} + \frac{b_0^2}{R_2 h} \right) \frac{w_0^2}{h^2} + \left(\frac{a_0^2}{R_1 h} + \frac{b_0^2}{R_2 h} \right)^2 \frac{w_0}{h} + \frac{24\Upsilon(\Phi - \Phi')}{h^2} \frac{w_0}{h} \quad (38)$$

where the membrane deformations are represented by a third degree polynomial, the bending deformations are represented by a linear function. Introducing the following non-dimensional parameters:

$$\bar{q} = \frac{3\Upsilon S^2 q}{\pi^2 h^3}, \quad \bar{w}_0 = \frac{w_0}{h}, \quad k_1 = \frac{a_0^2}{R_1 h} + \frac{b_0^2}{R_2 h}, \quad k_2 = \frac{24\Upsilon(\Phi - \Phi')}{h^2} \quad (39)$$

equation (38) can be rewritten as:

$$\bar{q} = 8\bar{w}_0^3 - 6k_1\bar{w}_0^2 + (k_1^2 + k_2)\bar{w}_0 \quad (40)$$

The displacements at the local maximum and minimum load can be found through:

$$\frac{\partial \bar{q}}{\partial \bar{w}_0} = 0 \Rightarrow 24\bar{w}_0^2 - 12k_1\bar{w}_0 + k_1^2 + k_2 = 0 \quad (41)$$

The localized snap-through buckling occurs, when equation (41) has two different rational roots:

$$k_1^2 > 2k_2 \quad (42)$$

$$\bar{w}_0 = \frac{k_1}{4} \left(1 \pm \sqrt{\frac{1}{3} - \frac{2k_2}{3k_1^2}} \right) \quad (43)$$

Substituting the two roots into equation (40), the critical buckling load and the minimum load after buckling can be obtained:

$$\bar{q}_{cr} = \frac{k_1^3}{4} \left[\frac{k_2}{k_1^2} \mp \left(\frac{1}{3} - \frac{2k_2}{3k_1^2} \right)^{\frac{3}{2}} \right] \quad (44)$$

In practice, these two loads may be considered as the upper and the lower bound of the critical buckling load, as a jump can take place from the first equilibrium path through the instability region to the second equilibrium path.

In Figure 3, the non-dimensional load \bar{q} is plotted against the non-dimensional deflection \bar{w}_0 for different k_1 and k_2 values. The left-hand graph is produced without bending deformations. When both R_1 and R_2 tend to infinity, the localized snap-through buckling does not occur, resulting in a monotonically increasing load deflection curve. For non-zero k_1 values, the load deflection curves can be divided into the following three parts that are characteristic of the snap-through buckling: the softening first equilibrium path, the instability region with a negative stiffness and the stable second equilibrium path. The right-hand graph is produced for general situations with both membrane and bending deformations. It shows that the snap-through buckling instability does not occur for small k_1 values, and the S-shaped curves are more precisely termed the geometrically non-linear behavior.

Up to now, the snap-through buckling problem has been discussed. For the buckling instability due to bifurcation, two different deformation mechanisms start to interact with each other because of the geometrical non-linearity, e.g. the in-plane compression leads to a sudden out-of-plane deflection in the classical Euler problem. As a matter of fact, the snap-through buckling has broadened the scope of the concept buckling, since this form of buckling is basically a limit point instability, where the membrane deformations start change from the compressive to the tensile state.

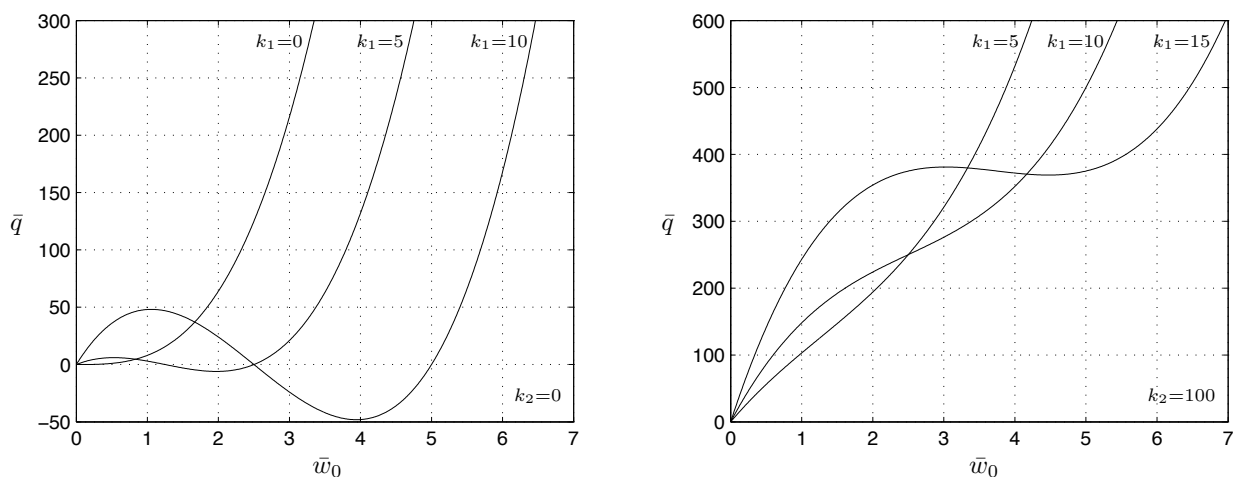


Figure 3. Non-dimensional load deflection curves

IV. Impact Induced Damage Development

When composite shell structures are subjected to low velocity impact, three major damage mechanisms that occur at the macromechanical scale are matrix cracking, internal delamination and fiber breakage. Focusing on the barely visible impact damage (BVID), the fiber breakage mode that plays an important role in the through penetration of laminates is left out of consideration. The matrix cracks that align parallel to the fibers and span the thickness of the plies lead to the elastic property degradation of the plies in the transverse or shear direction. The delaminations that break the base laminate into unsymmetrical sublaminates are known to dramatically reduce the laminate bending stiffness. Under the localized impact loading, the formation of the damage zone that contains an interconnected network of matrix cracks and delaminations implies the occurrence of a localized deformation field that is embedded within the global deformation field in the shell structure. On the basis of the global deformation field, a failure analysis can be performed for the matrix cracking in the individual plies. From the uncoupled localized deformation field, the strain energy released from the system can be calculated; and the energy balance for the delamination growth can then be established on the basis of the LEFM. In doing so, the existing plate impact model can be extended to a shell impact model, whereby the delamination is regarded as the primary failure mode and the matrix cracking as the secondary failure mode. Because of the highly localized nature of the phenomena, the remainder of this paper will make use of Donnell's theory in order to reduce the complexity of obtaining equations, while preserving acceptable accuracy.

A. Delamination Threshold Load

From the foregoing discussion in Section II, it is evident that a shell behaves like a plate, when the wavelength of the deformation pattern is sufficiently small. For this reason, the delamination threshold load that was derived for a quasi-isotropic plate is universally applicable for laminated composite structures, since the size of the initial delamination is by definition exceedingly small, and the bending stiffness matrix of a quasi-isotropic laminate has a general character. This means that the delamination threshold load P_{cr} of a cylindrical composite shell, can be calculated in a manner analogous to a flat plate:

$$P_{cr} = \sqrt{32\pi^2\alpha G_{IIC}\xi_{min}} \quad (45)$$

which is founded on the energy balance principle, which states that crack extension occurs when the energy available for crack growth is sufficient to overcome the resistance of the material. To start the calculation, the matrix cracks can be tentatively neglected. In equation (45), G_{IIC} is the critical mode II energy release rate of the unidirectional material, as the delamination growth is dominated by the shearing crack extension

mode. For the upper bound, α is equal to 1; for the lower bound, α depends on the Poisson's ratio of the laminate: $\alpha = (1 + \nu_{xy})/(3 + \nu_{xy})$. The parameter ξ_{min} is determined by solving the following minimization problem with respect to the delamination depth i in N possible interfaces and the orientation angle θ :

$$\begin{aligned} \text{minimize} \quad & \xi = \left(\frac{1}{\overline{D}_1 + \overline{D}_2} - \frac{1}{\overline{D}_0} \right)^{-1} \\ \text{subject to} \quad & i = 1, \dots, N \text{ for } 0 \leq \theta \leq \pi \end{aligned} \quad (46)$$

where \overline{D}_0 is the flexural rigidity for the undelaminated laminate, and $\overline{D}_1 + \overline{D}_2$ is the total flexural rigidity of the two delaminated sublaminates. More details on the calculation method are contained in Huang et al.¹.

B. Matrix Cracking Analysis

Consider a simply supported narrow cylindrical shell in the undamaged state, it is assumed that the shell does not undergo the snap-through buckling before the delamination threshold load; therefore, the deformations and stresses in the shell can be determined through a small deflection analysis. Since the concentrated point load leads to the stress singularity at the loading point, the impact load is supposed to be uniformly distributed over a circular Hertzian contact zone. As shown by Timoshenko and Woinowsky-Krieger²², the distributed load can be expressed in the form of a double Fourier series as follows:

$$q(x, y) = \sum_{m=1}^{\infty} \sum_{n=1}^{\infty} a_{mn} \sin \frac{m\pi x}{a} \sin \frac{n\pi y}{b} \quad (47)$$

$$a_{mn} = \frac{8P_{cr}}{abc\gamma_{mn}} J_1(\gamma_{mn}c) \sin \frac{m\pi x_0}{a} \sin \frac{n\pi y_0}{b} \quad \text{with} \quad \gamma_{mn} = \pi \sqrt{\frac{m^2}{a^2} + \frac{n^2}{b^2}} \quad (48)$$

where a and b are the length and width of the shell, the resultant load is taken as equal to the upper bound of the delamination threshold load P_{cr} , the center of the loading area is located at (x_0, y_0) , c is the contact radius, and $J_1(\gamma_{mn}c)$ is the Bessel function of the first kind with the argument $\gamma_{mn}c$. From the generalized equation of Donnell (20), it follows that:

$$w(x, y) = \sum_{m=1}^{\infty} \sum_{n=1}^{\infty} \frac{a_{mn}}{b_{mn}} \sin \frac{m\pi x}{a} \sin \frac{n\pi y}{b} \quad (49)$$

$$b_{mn} = \pi^4 \mathbb{D} + \frac{m^4}{a^4 R^2 \mathbb{S}} \quad (50)$$

where the parameters \mathbb{D} and \mathbb{S} are defined as:

$$\mathbb{D} = D_{11} \frac{m^4}{a^4} + 2H \frac{m^2 n^2}{a^2 b^2} + D_{22} \frac{n^4}{b^4}, \quad \mathbb{S} = S_{22} \frac{m^4}{a^4} + 2J \frac{m^2 n^2}{a^2 b^2} + S_{11} \frac{n^4}{b^4} \quad (51)$$

Substituting equation (49) into the linearized biharmonic membrane equation (19) gives:

$$\nabla_S^4 \phi = \frac{m^2 \pi^2}{a^2 R} \sum_{m=1}^{\infty} \sum_{n=1}^{\infty} \frac{a_{mn}}{b_{mn}} \sin \frac{m\pi x}{a} \sin \frac{n\pi y}{b} \quad (52)$$

The stress function ϕ can be obtained through direct integration:

$$\phi = \frac{m^2}{\pi^2 a^2 R S} \sum_{m=1}^{\infty} \sum_{n=1}^{\infty} \frac{a_{mn}}{b_{mn}} \sin \frac{m\pi x}{a} \sin \frac{n\pi y}{b} \quad (53)$$

Differentiating the displacement field w and the stress function ϕ with respect to the coordinates x and y , the principal stresses in an arbitrary k -th ply can be calculated by means of the CLT.

Lately a maximum strain energy based failure criterion has been developed for the intralaminar failures in the plies (see Huang²³). On the lamina level, the three fundamental failure modes are the longitudinal failure mode, the transverse failure mode and the shear failure mode. In point of fact, the longitudinal and shear failure mode can be excluded in the current analysis, as the corresponding stresses and strains in the plies usually remain beneath the critical values. Considering the transverse failure mode as a premature non-critical mode, it can be supposed that there is no interaction between the different failure modes. For a laminate with fiber dominated in-plane failure behavior, the maximum strain energy criterion can be simplified to the maximum stress criterion. The occurrence of transverse matrix cracks due to the combined bending and membrane stresses can be predicted on a ply-by-ply basis. After that, the transverse Young's modulus of the failed plies is reduced to zero. The delamination threshold load is recalculated by means of equations (45) and (46), resulting in the definitive delamination threshold load. In principle, an iterative loop leads to even higher accuracy. However, for many practical laminates, the improvement appears to be very limited; moreover, the predictor-corrector procedure gives a conservative prediction. In the further delamination propagation analysis, the effects of the stiffness degradation due to the matrix cracking are neglected, as the laminate bending stiffness becomes dominated by the multiple delaminations, while the laminate membrane stiffness is dominated by the fibers that remain intact.

C. Damage Zone Shape and Resultant Fracture Toughness

In this paragraph, the shape of the damage zone is determined through a linear deformation analysis of the near field in the vicinity of the impact point, and the resultant fracture toughness of multiple delaminations is proposed in a more general form in relation to the previous plate model. For this purpose, the damage zone is artificially extended in both longitudinal and circumferential direction to form a cylindrical shell of

sufficient size, and the impact load P is expressed in the form of a Fourier integral:

$$q(x, y) = \frac{P}{\pi^2 l^2} \int_0^\infty \int_0^\infty \cos \frac{\alpha x}{l} \cos \frac{\beta y}{l} d\alpha d\beta \quad (54)$$

where $\delta(x, y) = \frac{1}{\pi^2} \int_0^\infty \int_0^\infty \cos \alpha x \cos \beta y d\alpha d\beta$ is known as the Dirac delta function and l is an arbitrary characteristic length. In this study, l is taken as equal to the shell radius R . Substituting equation (54) into the generalized equation of Donnell (20), the following deflection field can be found:

$$w = \frac{PR^2}{\pi^2} \int_0^\infty \int_0^\infty g(\alpha, \beta) \cos \frac{\alpha x}{R} \cos \frac{\beta y}{R} d\alpha d\beta \quad (55)$$

where the function $g(\alpha, \beta)$ is defined as:

$$\frac{1}{g(\alpha, \beta)} = \mathbb{D}' + \frac{\alpha^4 R^2}{\mathbb{S}'}, \quad \mathbb{D}' = \tilde{D}_{11}\alpha^4 + 2\tilde{H}\alpha^2\beta^2 + \tilde{D}_{22}\beta^4, \quad \mathbb{S}' = S_{22}\alpha^4 + 2J\alpha^2\beta^2 + S_{11}\beta^4, \quad [\tilde{D}] = \sum_{i=1}^n [\tilde{D}_i^*] \quad (56)$$

where $[\tilde{D}_i^*]$ is the reduced bending stiffness matrix of the i -th delaminated sublaminates.

To eliminate the effects of boundary conditions on the local deformations, the long wavelength components are left out by taking the lower limits of the double integral as equal to 2 (see Łukasiewicz²⁴). The short wavelength components damp out rapidly as the distance from the loading point increases; therefore, the upper limits of the double integral can be taken as equal to 10. In brief, equation (55) can be evaluated in the manner of a mid-pass filter, with $\alpha_1 = \beta_1 = 2$ and $\alpha_2 = \beta_2 = 10$:

$$w = \frac{PR^2}{\pi^2} \int_{\beta_1}^{\beta_2} \int_{\alpha_1}^{\alpha_2} g(\alpha, \beta) \cos \frac{\alpha x}{R} \cos \frac{\beta y}{R} d\alpha d\beta \quad (57)$$

When the principal stiffness directions of the laminate are aligned with the longitudinal and circumferential axes of the shell, it appears that the contours of equal deflections are by approximation concentric ellipses that are symmetric with respect to the shell axes (see Figure 4). For an arbitrary ellipse, the semi-axes a_0

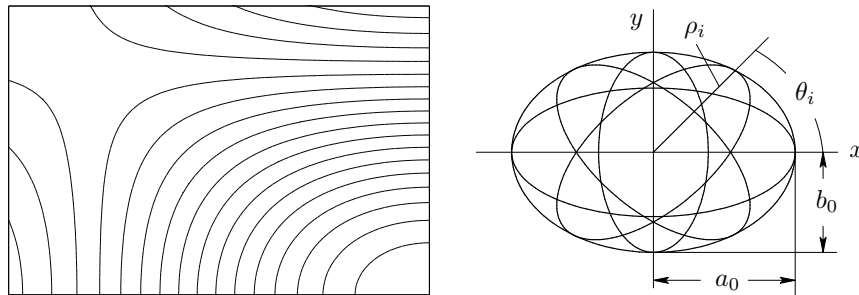


Figure 4. Typical equal deflection contours and idealized multiple delaminations

and b_0 satisfy the integral equation below:

$$\int_{\beta_1}^{\beta_2} \int_{\alpha_1}^{\alpha_2} g(\alpha, \beta) \left(\cos \frac{\alpha a_0}{R} - \cos \frac{\beta b_0}{R} \right) d\alpha d\beta = 0 \quad (58)$$

As there hold $a_0 \ll R$ and $b_0 \ll R$, the Taylor series expansion $\cos x = 1 - \frac{x^2}{2!} + \frac{x^4}{4!} - \frac{x^6}{6!} + \dots$ can be applied to obtain a closed-form solution of the ellipticity ratio λ_0 :

$$\lambda_0^2 = \frac{b_0^2}{a_0^2} = \frac{\int_{\beta_1}^{\beta_2} \int_{\alpha_1}^{\alpha_2} \alpha^2 g(\alpha, \beta) d\alpha d\beta}{\int_{\beta_1}^{\beta_2} \int_{\alpha_1}^{\alpha_2} \beta^2 g(\alpha, \beta) d\alpha d\beta} \quad (59)$$

The impact damage develops in the most efficient possible way, whereby the maximum strain energy release from the system is combined with the minimum fracture energy dissipation by the structure. Hence, it can be assumed that the external contours of the damage zone coincide with the equal deflection contours.

The resultant fracture toughness of the multiple delaminations can be calculated by assuming that the individual delaminations are elliptic and centered at the damage zone. Depending on which propagation direction leads to more bending energy release, the orientation angle θ_i of the i -th delamination is taken equal to the fiber orientation of the upper or lower adjacent ply. The ellipticity ratio λ_i for the i -th delamination is determined by the reduced bending stiffness constants of two adjacent sublaminates:

$$\lambda_i = \sqrt[4]{\frac{D_{22, i}^* + D_{22, i+1}^*}{D_{11, i}^* + D_{11, i+1}^*}} \quad (60)$$

The major axis ρ_i of the i -th delamination is given by:

$$\rho_i^2 = \left(\frac{\cos^2 \theta_i}{a_0^2} + \frac{\sin^2 \theta_i}{b_0^2} \right)^{-1} = \frac{a_0 b_0}{\lambda_0 \cos^2 \theta_i + \lambda_0^{-1} \sin^2 \theta_i} \quad (61)$$

The ratio between the area of the i -th delamination and the area of the damage zone is:

$$\eta_i = \frac{A_i}{S} = \frac{\lambda_i}{\lambda_0 \cos^2 \theta_i + \lambda_0^{-1} \sin^2 \theta_i} \quad (62)$$

The resultant critical energy release rate G_C for multiple delaminations becomes:

$$\sum_{i=1}^n A_i = S \sum_{i=1}^n \eta_i \Rightarrow G_C = G_{IIC} \sum_{i=1}^n \eta_i \quad (63)$$

It can be construed that G_C represents the total amount of energy dissipated per unit area of the damage zone.

D. Simplified Membrane Stiffnesses of Damage Zone

In contrast with the delamination threshold load, the delamination propagation load is strongly affected by the membrane behavior of the damage zone. It can be expected that the localized snap-through buckling occurs in the damage zone because of the significantly reduced bending stiffness. In case the shell curvature is such small that the localized snap-through buckling plays no part, the reader is referred to the previous flat plate model. For the concentrated point load, in principle, the $w = w_0(1 - \rho^2 + \rho^2 \ln \rho^2)$ type displacement field has to be substituted into the biharmonic membrane equation (6) to find an exact stress function ϕ . For the sake of mathematical convenience, the singular term $\ln \rho^2$ can be removed with the help of the Maclaurin series expansion $\ln x = (x - 1) - \frac{(x-1)^2}{2} + \frac{(x-1)^3}{3} - \frac{(x-1)^4}{4} + \dots$, $0 < x \leq 2$. In this way, approximations can be obtained in the form of the first order, second order, and so forth. It can be seen that the displacement field of the first order approximation $w \approx w_0(1 - \rho^2)^2$ corresponds to a clamped elliptic shell under uniformly distributed load. From a mechanics viewpoint, the $\rho^2 \ln \rho^2$ type singularity arises solely out of the idealization to the concentrated point load. Observe that the contact load is actually distributed in a small circular area at the center, an attempt can be made to calculate the membrane deformations by discarding the singular term. As the zero-th order Maclaurin approximation, the displacement field $w = w_0(1 - \rho^2)$ for a simply supported elliptic shell under uniformly distributed load is used to evaluate the membrane stiffness of the elliptic shell.

Setting $R_1 \rightarrow \infty$ and $R_2 = R$, the expression for the membrane energy (31) reduces to:

$$U_m = \frac{\pi^2 w_0^2}{12S\Upsilon} \left(\frac{b_0^2}{R} - 2w_0 \right)^2 \quad (64)$$

Discarding the higher order terms yields the linearized prebuckling membrane stiffness of the damage zone:

$$U'_m = \frac{\pi^2 b_0^4 w_0^2}{12S\Upsilon R^2} \Rightarrow K'_m = \frac{\partial^2 U'_m}{\partial w_0^2} = \frac{\pi^2 b_0^4}{6S\Upsilon R^2} \quad (65)$$

For the postbuckling membrane stiffness, it can be assumed that the middle surface is not stretched in the circumferential direction, the maximum deflection w_0 can be determined by mirroring the shell middle surface (see Figure 5). With the help of the Taylor series expansion $\cos x = 1 - \frac{x^2}{2!} + \frac{x^4}{4!} - \frac{x^6}{6!} + \dots$, the following equation can be obtained:

$$w_0 = 2R \left(1 - \cos \frac{b_0}{R} \right) \approx \frac{b_0^2}{R} \quad (66)$$

Substituting equation (66) into equation (64), the membrane energy in the damage zone becomes:

$$U_m'' = \frac{\pi^2 w_0^4}{12S\Upsilon} \quad (67)$$

resulting in the following simplified postbuckling membrane stiffness:

$$K_m'' = \frac{\partial^2 U_m''}{\partial w_0^2} = \frac{\pi^2 w_0^2}{S\Upsilon} \quad (68)$$

By approximating the parabola $w_0 = 1 - y^2/b_0^2$ with an arc of the radius R , the length calculation of the parabola through integration is avoided, and the relation between w_0 and b_0 is therefore simplified to a great extent. The practical advantage thereof is that the postbuckling membrane stiffness K_m'' can be calculated through a simple equation with a reasonable accuracy.

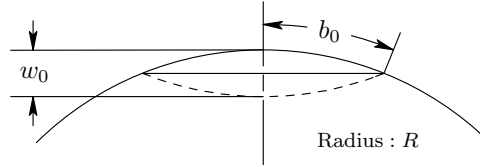


Figure 5. Isometric transformation

E. Energy Balance and Damage Area

Referring to Huang et al.¹, the energy balance equation for the propagation of the multiple delaminations is given by:

$$G_c = \frac{P^2}{32\pi^2} \left(\frac{1}{\sum_{i=1}^{n+1} \bar{D}_i + \Psi_2} - \frac{1}{\bar{D}_0 + \Psi_1} \right) \quad (69)$$

where Ψ_1 and Ψ_2 are related to the prebuckling and postbuckling membrane stiffnesses of the damage zone K_m' and K_m'' , respectively. Using the scaling factor $16\pi^2/S$ from the bending stiffness, Ψ_1 and Ψ_2 become:

$$\Psi_1 = \frac{b_0^4}{96\Upsilon R^2}, \quad \Psi_2 = \frac{w_0^2}{16\Upsilon} \quad (70)$$

As $\sum_{i=1}^{n+1} \bar{D}_i + \Psi_2 \ll \bar{D}_0 + \Psi_1$ and $\sum_{i=1}^{n+1} \bar{D}_i \ll \Psi_2$, equation (69) can be reduced to a linear equation:

$$P = \sqrt{2\pi^2\Upsilon^{-1}G_c} w_0 \quad (71)$$

The G_c value can be determined through the following minimization problem, which combines the maximum bending stiffness reduction with the minimum delamination propagation load:

$$\begin{aligned} \text{minimize } \Lambda &= \frac{\sum_{i=1}^{n+1} \bar{D}_i}{\bar{D}_0} \sqrt{\frac{\hat{\Upsilon}}{\Upsilon} \sum_{i=1}^n \eta_i} \\ \text{subject to } n &= 1, \dots, N \end{aligned} \quad (72)$$

where n is the number of delaminations and N is the number of interfaces. The terms \bar{D}_0 and $\hat{\Upsilon}$ are used to make the objective function Λ dimensionless, where the parameter $\hat{\Upsilon}$ is defined as $\hat{\Upsilon} = (3S_{11} + 2J + 3S_{22})/8$.

Superposed with the global shell deformations, the loading part of the load deflection curve becomes:

$$P - P_{cr} = \frac{\delta - \delta_{cr}}{C_p} \quad \text{with } C_p = C_u + \sqrt{2\pi^2 \Upsilon^{-1} G_c} \quad (73)$$

where P is the impact load, P_{cr} is the delamination threshold load, δ is the total target deflection, C_u is the undamaged target compliance and C_p is the compliance of the delamination propagation curve. On the basis of equation (73), a similar load deflection curve can be constructed for the cylindrical shell as in the case of the flat plate; therefore, the relations between the damage area S and the impactor kinetic energy E_k as well as the peak impact load P_{max} from the flat plate model remain applicable to the cylindrical shell:

$$S = \frac{P_{max}^2 - P_{cr}^2}{\sqrt{8\pi^2 \Upsilon^{-1} G_c^3}} \quad (74)$$

$$S = \frac{\Gamma}{G_c} H(E_k - E_{cr})(E_k - E_{cr}) \quad \text{with } \Gamma = 1 - \frac{C_u}{C_p} \quad (75)$$

where Γ is the impact energy transfer factor, and H is the Heaviside step function.

Up to this point, the impact model has been extended from a quasi-isotropic flat plate to a cylindrical shell with a more general lay-up. Following the same development philosophy, the model can be further extended to a doubly curved shell or even a arbitrarily shaped shell. It is clear that various uncoupling techniques have played an important role in achieving an efficient model: Selecting a symmetrical and balanced lay-up or prescribing the out-of-plane displacement fields in a symmetrical way, the effects of the laminate couplings are eliminated as much as possible. Modifying the boundary conditions, the localized deformation field is uncoupled from the global deformation field. Dealing with the coupled membrane and bending deformations, the membrane effects are neglected in the delamination threshold load, and the bending effects are neglected in the delamination propagation load. For the complicated coupling effects, one may resort to the numerical methods such as the finite element method or the finite difference method.

V. Damage Tolerance Analysis

The ultimate strength of cylindrical composite shells under axial compression is closely connected with various buckling mechanisms, which occur in a local or global manner. In this section, the critical stresses are discussed for different buckling modes, followed by the postbuckling behavior of a squared cylindrical shell. The residual compression strength is determined through a synthesis of the fundamental failure modes. To elucidate the basic physical principles behind the complex buckling and postbuckling phenomena, the equations are presented on the basis of an isotropic material. At the end, the buckling and postbuckling solutions will be given for a symmetrical and balanced laminate. As the succinct isotropic equations can be easily generalized to solve similar anisotropic problems, the detailed derivation of the anisotropic equations will be omitted. The concept damage tolerance, as used in the context of this discussion, relates to the reduction of the compression performance of cylindrical shell structures due to the presence of the BVID.

A. Localized Snap-through Due to Axial Compression

When a perfect isotropic cylindrical shell buckles into a symmetrical form in Figure 6, according to Lorenz¹⁷ the critical buckling stress would be:

$$\sigma_{cr} = \frac{Eh}{\sqrt{3(1-\nu^2)}R}, \quad \sigma_{cr} \approx 0.612 \frac{Eh}{R} \quad \text{for } \nu = \frac{1}{3} \quad (76)$$

In Timoshenko and Gere¹⁸, the following empirical formula can be found, where the critical stress is roughly halved:

$$\sigma_{cr} = E \frac{0.6 \frac{h}{R} - 10^{-7} \frac{R}{h}}{1 + 0.004 \frac{E}{\sigma_{YP}}}, \quad \sigma_{cr} \approx 0.291 \frac{Eh}{R} \quad \text{for duralumin} \quad (77)$$

For the material duralumin, the ratio between the Young's modulus and the yield stress E/σ_{YP} is equal to 265. The simplified formula is obtained by neglecting the term $10^{-7}R/h$.

On the basis of the results presented in Section III, it is comprehensible that the localized snap-through mode that involves a lower level of the deformation energy should lead to a lower buckling stress than the symmetrical mode. In Figure 6, the localized snap-through mode is sketched in an isolated manner, whereas the idealized overall buckling deformation pattern consists of many of the identical elliptic regions that are packed in a regular array. Under the uniform axial compression, it can be expected that the axes of the elliptic regions are aligned with the longitudinal and circumferential directions of the cylindrical shell. Using the energy equation (36), it can be proven that the localized deformation field becomes energetically more efficient, when the wavelength of the deformation pattern becomes smaller in the circumferential direction, i.e. the utilization of Donnell's theory in the buckling calculations is justified. Neglecting the term Φ' and

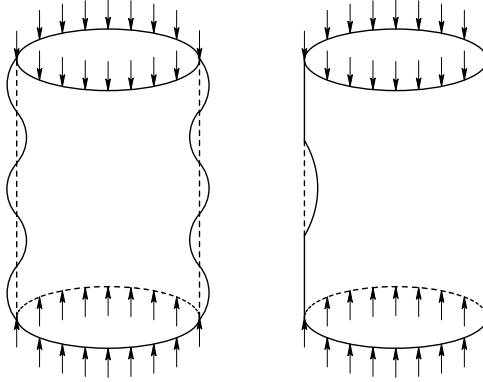


Figure 6. Symmetrical and localized snap-through mode

linearizing the membrane energy at the point $w_0 = 0$, the total strain energy in the localized quadratic deflection field becomes:

$$\Delta U = \frac{\pi^2 b_0^4 w_0^2}{12S\Upsilon R^2} + \frac{2\pi^2 \Phi w_0^2}{S} \quad (78)$$

Using the isometric transformation, the linearization at the point $w_0 = b_0^2/R$ provides the same equation, although the w_0 value is different. The snap-through instability implies that the buckling stress has an upper and a lower bound corresponding to the local maximum and minimum on the non-linear equilibrium path. As a result of the linearization, the maximum and minimum points lead to the same buckling stress. Due to the quadratic deflections, the work done by the membrane forces is:

$$\Delta T = -\frac{N_x}{2} \iint_S \left(\frac{\partial w}{\partial x} \right)^2 dS = -\frac{\pi b_0 N_x w_0^2}{2a_0} \quad (79)$$

where the minus sign before the integral is added so that ΔT can be expressed as a positive value. According to the energy based buckling criterion:

$$\Delta U = \Delta T \quad (80)$$

the magnitude of the critical buckling load N_{cr} for the localized snap-through mode becomes:

$$N_{cr} = \frac{b_0^2}{6\Upsilon R^2} + \frac{4\Phi}{b_0^2} \quad (81)$$

By requiring $\partial N_{cr}/\partial b_0 = 0$ or using the inequality $\alpha + \beta \geq 2\sqrt{\alpha\beta}$, equation (81) can be simplified to:

$$b_0^4 = 24\Upsilon\Phi R^2 \Rightarrow N_{cr} \geq \frac{1}{R} \sqrt{\frac{8\Phi}{3\Upsilon}} \quad (82)$$

Physically this means that the membrane energy is equal to the bending energy at the bifurcation point.

For an isotropic material, equation (82) can be rewritten as:

$$N_{cr} \geq \frac{Eh^2}{R} \sqrt{\frac{2}{9(1-\nu^2)} \frac{\lambda_0^2 + 2\nu + \lambda_0^{-2}}{3\lambda_0^2 + 2 + 3\lambda_0^{-2}}} \quad (83)$$

To obtain the lowest N_{cr} , equation (83) has to further minimized with respect to the ellipticity ratio λ_0 . It turns out that the minimum of N_{cr} is associated with a circular buckled zone:

$$\frac{\partial N_{cr}}{\partial \lambda_0} = 0 \Rightarrow \lambda_0 = 1 \Rightarrow N_{cr} \geq \frac{Eh^2}{\sqrt{18(1-\nu)}R} \quad (84)$$

From equation (82), it follows that the following relation between b_0 and Rh is valid:

$$\frac{b_0^2}{Rh} = \sqrt{\frac{32}{1-\nu}} \quad (85)$$

For $\nu = 1/3$, the magnitude of the critical buckling stress σ_{cr} is:

$$\sigma_{cr} = \frac{N_{cr}}{h} \geq \frac{Eh}{2\sqrt{3}R} \approx 0.289 \frac{Eh}{R} \quad (86)$$

It can be seen that equation (86) agrees well with equation (77). This confirms that the localized snap-through mode is the lowest buckling mode. If $\nu = 1/3$, N_{cr} becomes independent of λ_0 ; therefore, λ_0 can not be determined through equation (83), but through equation (82) by minimizing b_0 with respect to λ_0 . Also in this specific case, there holds: $\lambda_0 = 1$. As is known, the buckling strength of an unstiffened cylindrical shell can be considered as its ultimate compression strength because of the unstable postbuckling state.

B. Global Buckling of Cylindrical Panel

This paragraph is concerned with the buckling behavior of a cylindrical shell containing an elliptic zone that is representative of the BVID. It is assumed that the shell within the damage zone behaves like a perfectly flexible membrane. As shown in Figure 7, the shell is simply supported along two generators and two circular edges and uniformly compressed in the axial direction. The length and the curved width of the shell are a and b , respectively. It is supposed that the damage zone is small compared with the shell radius R .

On the analogy of Navier's solution for a rectangular flat plate, it is supposed that the shape of the deflected surface can be represented by the following double trigonometric function:

$$w = w_0 \sin \frac{m\pi x}{a} \sin \frac{n\pi y}{b} \quad (87)$$

where m and n are the half-wave numbers. Using the calculation method presented in Huang et al.¹, the

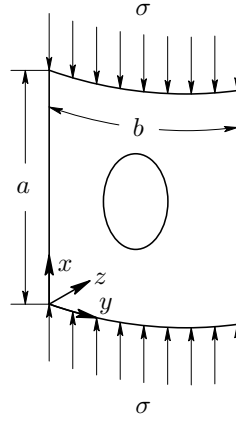


Figure 7. Curved panel under compression

bending energy in the displacement field w is found to be:

$$\Delta U_b = \frac{\pi^4 \zeta ab D w_0^2}{8} \left(\frac{m^2}{a^2} + \frac{n^2}{b^2} \right)^2, \quad \zeta = 1 - \frac{4}{ab} \iint_S \left(\sin \frac{m\pi x}{a} \sin \frac{n\pi y}{b} \right)^2 dS \quad (88)$$

where ζ is the energy reduction factor. The integration is performed over the area S of the damage zone.

Using equation (53), the membrane energy in the displacement field w can be expressed as:

$$\phi = \frac{m^2 E h w_0}{\pi^2 a^2 R} \left(\frac{m^2}{a^2} + \frac{n^2}{b^2} \right)^{-2} \sin \frac{m\pi x}{a} \sin \frac{n\pi y}{b} \Rightarrow \Delta U_m = \frac{\zeta m^4 b E h w_0^2}{8 a^3 R^2} \left(\frac{m^2}{a^2} + \frac{n^2}{b^2} \right)^{-2} \quad (89)$$

Reducing equation (81) to $N'_{cr} = b_0^2 / (6\Upsilon R^2)$, it can be seen that the damage zone undergoes the localized snap-through buckling in a very early stage of the compression process. Neglecting the contribution of the membrane energy in the damage zone, the total strain energy in the displacement field w becomes:

$$\Delta U = \zeta \left[\frac{\pi^4 ab D w_0^2}{8} \left(\frac{m^2}{a^2} + \frac{n^2}{b^2} \right)^2 + \frac{m^4 b E h w_0^2}{8 a^3 R^2} \left(\frac{m^2}{a^2} + \frac{n^2}{b^2} \right)^{-2} \right] \quad (90)$$

To obtain a conservative prediction, the work done by the membrane forces due to the lateral deflections is calculated as follows:

$$\Delta T = -\frac{N_x}{2} \int_0^b \int_0^a \left(\frac{\partial w}{\partial x} \right)^2 dx dy = -\frac{\pi^2 m^2 b N_x w_0^2}{8a} \quad (91)$$

From the energy principle it follows that the magnitude of the critical buckling stress is:

$$\sigma_{cr} = \zeta \left[\frac{\pi^2 a^2 D}{m^2 h} \left(\frac{m^2}{a^2} + \frac{n^2}{b^2} \right)^2 + \frac{m^2 E}{\pi^2 a^2 R^2} \left(\frac{m^2}{a^2} + \frac{n^2}{b^2} \right)^{-2} \right] \quad (92)$$

It can be seen that the buckling resistance of a cylindrical shell comprises a bending term and a membrane term, where the bending term is dominant for a large R .

Using again the inequality $\alpha + \beta \geq 2\sqrt{\alpha\beta}$, the following is found for the symmetrical mode:

$$\sigma_{cr} \geq 2\zeta \sqrt{\frac{DE}{hR^2}} = \frac{\zeta Eh}{\sqrt{3(1-\nu^2)}R} \quad (93)$$

The minimum occurs under the condition $\alpha = \beta$ or $U_m = U_b$. That is:

$$m^2 - 2K \frac{a}{b} m + n^2 \frac{a^2}{b^2} = 0 \quad (94)$$

where the parameter K is defined as:

$$K = \frac{\sqrt[4]{12(1-\nu^2)}}{2\pi} \frac{b}{\sqrt{Rh}} \quad (95)$$

The rational roots of the quadratic equation above are:

$$m = \frac{a}{b} \left(K \pm \sqrt{K^2 - n^2} \right) \quad \text{if } K \geq n \quad (96)$$

When there is one half-wave in the circumferential direction, the integer n reaches its minimum value of 1. Hence, the symmetrical mode occurs only if the following condition is satisfied: $K \geq 1$.

For $K < 1$, the minimization of equation (92) leads to a square buckle and the lowest critical buckling stress is:

$$\frac{\partial \sigma_{cr}}{\partial m} = 0 \Rightarrow m = \frac{a}{b} \Rightarrow \sigma_{cr} = \zeta E \left[\frac{\pi^2 h^2}{3(1-\nu^2)b^2} + \frac{b^2}{4\pi^2 R^2} \right] = \frac{\zeta \pi^2 (1+K^4) E h^2}{3(1-\nu^2)b^2} \quad (97)$$

where the longitudinal wave is located in relation to the damage zone in such a way that the factor ζ reaches its minimum. It can be construed that equation (97) describes the critical buckling stress of the narrow shell mode, in which the buckling behavior of a cylindrical shell resembles that of a rectangular plate. This explains why the bending energy prevails over the membrane energy.

On the basis of equation (85), the localized snap-through buckling occurs under the following condition:

$$K \geq \frac{\sqrt[4]{24(1+\nu)}}{\pi} \quad (98)$$

If $\nu = 1/3$, then $K \geq 0.757$. As the localized snap-through mode occurs at $K \geq 0.757$, the symmetrical mode with $K \geq 1$ does not occur under normal circumstances, the narrow shell mode occurs in the reduced range of $0 \leq K < \sqrt[4]{24(1+\nu)}/\pi$. From this analysis, it is clear that Donnell's theory is applicable in the most shell buckling calculations. When a long cylindrical shell buckles in the manner of a slender beam, Donnell's theory becomes inaccurate, and one may employ Love's theory or revert to the Euler buckling theory.

C. Postbuckling Analysis of Cylindrical Shell

Recall the cylindrical shell in Figure (7), the length and the curved width are now both equal to a , the curvature parameter K ranges from 0 to $\sqrt[4]{24(1+\nu)}/\pi$, and the damage zone is set aside for convenience. The compression loads are transmitted to the shell via the two horizontal edges by two rigid blocks. The two vertical edges that are allowed to move freely in the in-plane directions remain straight during the deformations. During the analysis, the Poisson's ratio ν of the material is taken as equal to 1/3.

Using a curvilinear coordinate system $x-y$ at the center of the shell, the out-of-plane displacement field w from equation (87) is rewritten as:

$$w = w_0 \cos \frac{\pi x}{a} \cos \frac{\pi y}{a} \quad (99)$$

With regard to the membrane deformations, the stress function ϕ that satisfies the boundary conditions consists of five parts:

$$\phi = \phi_1 + \phi_2 + \phi'_2 + \phi_3 + \phi'_3 \quad (100)$$

The stress function ϕ_1 that represents the forced in-plane response to the out-of-plane displacement w can be obtained by substituting equation (99) into the non-linear biharmonic membrane equation (6):

$$\nabla^4 \phi_1 = \frac{\pi^2 E h w_0}{a^2 R} \cos \frac{\pi x}{a} \cos \frac{\pi y}{a} - \frac{\pi^4 E h w_0^2}{2a^4} \left(\cos \frac{2\pi x}{a} + \cos \frac{2\pi y}{a} \right) \quad (101)$$

$$\phi_1 = \frac{a^2 E h w_0}{4\pi^2 R} \cos \frac{\pi x}{a} \cos \frac{\pi y}{a} - \frac{E h w_0^2}{32} \left(\cos \frac{2\pi x}{a} + \cos \frac{2\pi y}{a} \right) \quad (102)$$

Substituting w and ϕ_1 into equations (3) and (4), the axial displacement u_1 at $x = a/2$ and the circumferential displacement v_1 at $y = a/2$ become:

$$u_1 = -\frac{\pi^2 w_0^2}{16a} - \frac{a w_0}{6\pi R} \cos \frac{\pi y}{a}, \quad v_1 = -\frac{\pi^2 w_0^2}{16a} + \frac{5a w_0}{6\pi R} \cos \frac{\pi x}{a} \quad (103)$$

To nullify the cosine component in u_1 , the stress function ϕ_2 is introduced, which leads merely to in-plane deformations:

$$\phi_2 = f(x) \cos \frac{\pi y}{a} \quad (104)$$

Substituting ϕ_2 into the biharmonic membrane equation (6) gives:

$$\nabla^4 \phi_2 = 0 \Rightarrow \frac{d^4 f}{dx^4} - 2\frac{\pi^2}{a^2} \frac{d^2 f}{dx^2} + \frac{\pi^4}{a^4} f = 0 \quad (105)$$

Referring to Timoshenko and Goodier²⁵, the general solution of the differential equation (105) is given by:

$$f = C_1 \cosh \frac{\pi x}{a} + C_2 \sinh \frac{\pi x}{a} + C_3 x \cosh \frac{\pi x}{a} + C_4 x \sinh \frac{\pi x}{a} \quad (106)$$

Because of the symmetry, the C_2 and C_3 terms that contain odd functions should vanish. On the basis of the Taylor series expansions $\cosh x = 1 + \frac{x^2}{2!} + \frac{x^4}{4!} + \frac{x^6}{6!} + \dots$ and $\sinh x = x + \frac{x^3}{3!} + \frac{x^5}{5!} + \frac{x^7}{7!} + \dots$, the term $C_4 x \sinh(\pi x/a)$ has a similar behavior as the higher order terms of $C_1 \cosh(\pi x/a)$. It can be seen that the first order term of $C_1 \cosh(\pi x/a)$ corresponds to the intended membrane stress distribution with $N_x = -C_1 \pi^2/a^2 \cos(\pi y/a)$ and $N_y = 0$. Discarding the higher order terms that do not satisfy the boundary conditions, ϕ_2 becomes:

$$\phi_2 = C_1 \cos \frac{\pi y}{a} \quad (107)$$

The accompanying displacement u_2 for the edge $x = a/2$ is:

$$u_2 = -\frac{\pi^2 C_1}{2aEh} \cos \frac{\pi y}{a} \quad (108)$$

The constant C_1 is determined by comparing u_1 with u_2 :

$$u_1 + u_2 \equiv -\frac{\pi^2 w_0^2}{16a} \Rightarrow C_1 = -\frac{a^2 E h w_0}{3\pi^3 R} \quad (109)$$

The stress function ϕ_3 that corresponds with the remaining uniform axial compression is:

$$\phi_3 = \frac{Eh}{2a} \left(\frac{\pi^2 w_0^2}{8a} - \delta \right) y^2 \quad (110)$$

where δ is the total end shortening of the shell. The stress functions $\phi'_2(x)$ and $\phi'_3(x)$ are of the same form as $\phi_2(y)$ and $\phi_3(y)$. Using ϕ'_2 , the cosine component in v_1 is nullified. With ϕ'_3 , the resulting forces along the vertical edges can be adjusted to 0; therefore, $\phi'_2 + \phi'_3$ does not produce a contraction in the axial direction. As the following relations are valid: $\partial^2 \phi'_2/\partial y^2 = 0$ and $\partial^2 \phi'_3/\partial y^2 = 0$, there is no need to derive the exact expressions of ϕ'_2 and ϕ'_3 in the current analysis.

The strain energy that is associated with the displacement field w and the stress function ϕ_1 is given by:

$$\Delta U = \frac{\pi^4 E h w_0^4}{128 a^2} - \frac{E h w_0^3}{18 R} + \frac{a^2 E h w_0^2}{32 R^2} + \frac{3 \pi^4 E h^3 w_0^2}{64 a^2} \quad (111)$$

Using the superposed stress function ϕ , the work done by the axial membrane forces due to the displacement

field w can be calculated as follows:

$$\Delta T = -\frac{1}{2} \int_{-\frac{a}{2}}^{\frac{a}{2}} \int_{-\frac{a}{2}}^{\frac{a}{2}} \frac{\partial^2 \phi}{\partial y^2} \left(\frac{\partial w}{\partial x} \right)^2 dx dy = -\frac{3\pi^4 E h w_0^4}{128 a^2} + \frac{\pi^2 E h \delta w_0^2}{8 a} \quad (112)$$

On the basis of the energy balance principle, the following relationship can be derived between the overall compressive strain ε and the maximum deflection w_0 :

$$\Delta U = \Delta T \Rightarrow \varepsilon = \frac{\delta}{a} = \frac{\pi^2 w_0^2}{4 a^2} - \frac{4 w_0}{9 \pi^2 R} + \underbrace{\frac{a^2}{4 \pi^2 R^2} + \frac{3 \pi^2 h^2}{8 a^2}}_{\varepsilon_{cr}} \quad (113)$$

in which the critical buckling strain ε_{cr} can be retrieved. For the stress function ϕ , it follows that the total compressive load in its non-dimensional form is given by:

$$\bar{N} = -\frac{1}{E h a} \int_{-\frac{a}{2}}^{\frac{a}{2}} \frac{\partial^2 \phi}{\partial y^2} dy, \quad x = \frac{a}{2} \Rightarrow \bar{N} = \varepsilon - \frac{\pi^2 w_0^2}{8 a^2} - \frac{2 w_0}{3 \pi^2 R} \quad (114)$$

For the critical buckling load, the following holds true: $\bar{N}_{cr} = \varepsilon_{cr}$. To construct the postbuckling curve, equations (113) and (114) can be rewritten as:

$$\varepsilon - \varepsilon_{cr} = \frac{\pi^2 w_0^2}{4 a^2} - \frac{4 w_0}{9 \pi^2 R}, \quad \bar{N} - \bar{N}_{cr} = \frac{\pi^2 w_0^2}{8 a^2} - \frac{10 w_0}{9 \pi^2 R} \quad (115)$$

where w_0 can be varied between 0 and a distance several times as large as the shell thickness h . The postbuckling curve ends at the point when the maximum stress level in the shell reaches the compression strength of the material σ_m . In the buckled configuration, the maximum compressive stresses are located at the vertical edges. Hence, the maximum end shortening can be calculated as follows:

$$\frac{\delta_{\max}}{a} = \frac{\sigma_m}{E} \quad (116)$$

Using equations (113) and (114), δ_{\max} can be further converted to the maximum overall strain ε_{\max} and the maximum applied stress σ_{\max} .

In Figure 8, the load deflection curves are plotted for a square flat plate and two cylindrical shells. To demonstrate the initial postbuckling behavior, \bar{N} and ε are normalized with respect to the non-dimensional buckling stress \bar{N}_{cr}^p and strain ε_{cr}^p of the flat plate. For the complete postbuckling range, \bar{N} and ε are normalized with respect to their own \bar{N}_{cr} and ε_{cr} , so that the different curves do not intersect with each other. Without the plastic deformations, the flat plate exhibits a linear postbuckling behavior, where the non-dimensional tangent stiffness is equal to 1/2. In this case, the current model gives the same result as Koiter's initial postbuckling theory, with which the slope and the curvature of the second equilibrium path

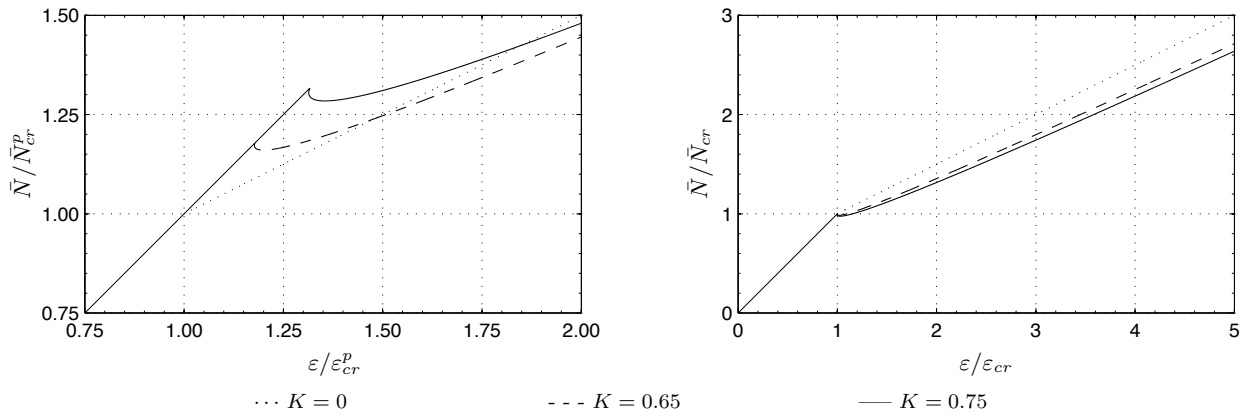


Figure 8. Normalized load deflection curves ($h = 1$ mm, $a = 200$ mm)

at the bifurcation point can be determined through a higher order linearization. For the cylindrical shells, the reversal of curvature in the circumferential direction manifests itself in the transient effect whereby the postbuckling curves first decrease and subsequently increase with the increasing overall strain. In theory, the initial postbuckling state of the narrow shell mode is unstable, unless the shell radius becomes infinite. In practice, such small-scale instability can be avoided through a variety of creative solutions, e.g. through the nonlinear deformation behavior of the polymer matrix, by permitting a minimized initial deflection or even using a smart structure concept with piezoelectric sensors and actuators. In the region far beyond the bifurcation point, the applied load is virtually linearly related to the in-plane deflection.

D. Failure Mode Synthesis

If the final collapse of an impact damaged cylindrical shell as shown in Figure (7) is controlled by the material failure mode, the residual compression strength can be calculated as follows:

$$\sigma_{\max}^* = \left(1 - \frac{\tilde{b}}{b}\right) \sigma_m \quad (117)$$

where \tilde{b} is the curved damage zone width. The compressive strength σ_m of a laminate can be calculated through the progressive damage analysis (see Huang²³). From the damage mechanics viewpoint, the notch insensitivity can be construed as sort of ideally plastic behavior of the laminate, i.e. the compressive stress in the laminate remains on a constant level of σ_m beyond the fiber failure. After the localized snap-through buckling, the damage zone can be treated as a cutout. The stress concentration around the damage zone initially plays a role in the stress distribution in the shell. With the increasing compression load, the damage starts to propagate over the smallest cross-section in the undamaged shell portion. In this way, a uniform stress distribution is gradually developed in the extended damage zone and the shell reaches the maximum load-carrying capacity, resulting in the simple linear relationship above. For the notch sensitive cases, the

mechanisms for damage progression and accumulation warrant closer investigation; a few models involving the finite element method appear to be available in the literature (see e.g. Matthews et al.²⁶).

The opposite situation is that the impact damaged cylindrical shell buckles before the material failure. The transition from the controlled postbuckling behavior to the highly unstable postbuckling behavior occurs at the point $K = \sqrt[4]{24(1+\nu)}/\pi$, where the narrow shell mode is taken over by the localized snap-through mode. Combining the two buckling modes with the material compression failure mode, the residual strength of the impact damaged cylindrical shell can be expressed as:

$$\sigma_{ult} = \begin{cases} \min(\sigma_{\max}^*, \sigma_{\max}) & \text{if } K < \sqrt[4]{24(1+\nu)}/\pi \\ \min(\sigma_{\max}^*, \sigma_{cr}) & \text{if } K \geq \sqrt[4]{24(1+\nu)}/\pi \end{cases} \quad (118)$$

where σ_{\max} is the postbuckling strength of the narrow shell mode and σ_{cr} the critical buckling strength of the localized snap-through mode. For an optimal accuracy of σ_{\max} , the weakening effects of the damage zone can be taken into account in the postbuckling analysis in an analogous way as the buckling analysis.

E. Anisotropic Stability Equations

With a thorough understanding of the underlying physics, it is a straightforward task to perform the damage tolerance analysis of an anisotropic shell by following the same calculation procedures as in the previous paragraphs. For the sake of brevity, the key equations that require refinements are summarized here.

When a cylindrical shell buckles in the localized snap-through mode, the critical load amplitude N_{cr} is given by equation (82). In the anisotropic case, equation (84) has to be generalized to:

$$\frac{\partial N_{cr}}{\partial \lambda_0} = 0 \Rightarrow (D_{11}J - 3D_{12}S_{22})\lambda_0^4 + 3(D_{11}S_{11} - D_{22}S_{22})\lambda_0^2 + (3D_{12}S_{11} - D_{22}J) = 0 \quad (119)$$

It can be seen that the buckling deformation pattern and the extensional and bending stiffnesses are coupled to each other in a rather complicated way.

If the narrow shell mode occurs, the anisotropic critical buckling load N_{cr} takes the following form:

$$N_{cr} = \zeta \left(\frac{\pi^2 a^2 \mathbb{D}}{m^2} + \frac{m^2}{\pi^2 a^2 R^2 \mathbb{S}} \right) \quad (120)$$

As $n = 1$, equation (120) is minimized with respect to m (For clarity, \mathbb{D} and \mathbb{S} are functions of m). If the bending term is much larger than the membrane term or there holds: $\frac{D_{22}}{D_{11}} \approx \frac{S_{22}}{S_{11}}$, m becomes equal to $\frac{a}{b} \sqrt[4]{\frac{D_{22}}{D_{11}}}$; otherwise, the equation $\frac{\partial N_{cr}}{\partial m} = 0$ can be solved using a numerical root finder. When the shell is isotropic and perfect, equation (120) reduces to the buckling solution in Timoshenko and Gere¹⁸. When the

shell radius R goes to infinity, equation (120) reduces to the buckling solution of rectangular flat plates in Huang et al.¹, where the bending stiffness of the damage zone is entirely neglected.

Consider a rectangular cylindrical shell, the anisotropic postbuckling analysis is carried out on the basis of the following out-of-plane displacement field:

$$w = w_0 \cos \frac{\pi x}{a} \cos \frac{\pi y}{b} \quad (121)$$

The stress functions that describe the membrane deformations are given by:

$$\phi_1 = \frac{b^2 w_0}{\pi^2 R Z} \cos \frac{\pi x}{a} \cos \frac{\pi y}{b} - \frac{a^2 w_0^2}{32 b^2 S_{22}} \cos \frac{2\pi x}{a} - \frac{b^2 w_0^2}{32 a^2 S_{11}} \cos \frac{2\pi y}{b} \quad (122)$$

$$\phi_2 = -\frac{2b^2 w_0}{\pi^3 R Z} \left(1 + \frac{b^2 S_{12}}{a^2 S_{11}} \right) \cos \frac{2\pi y}{b} \quad (123)$$

$$\phi_3 = \frac{1}{2a S_{22}} \left(\frac{\pi^2 w_0^2}{8a} - \delta \right) y^2 \quad (124)$$

where the parameter Z is defined as:

$$Z = \frac{b^2}{a^2} S_{22} + 2J + \frac{a^2}{b^2} S_{11} \quad (125)$$

The generalized relationships between ε , w_0 and \bar{N} are as follows:

$$\varepsilon = \frac{\pi^2 w_0^2}{16a^2} \left(2 + \frac{a^4}{2b^4} + \frac{3S_{22}}{2S_{11}} \right) - \frac{8S_{22}w_0}{\pi^2 R Z} \left(\frac{1}{9} - \frac{b^2 S_{12}}{2a^2 S_{11}} + \frac{a^2 S_{12}}{6b^2 S_{22}} \right) + \varepsilon_{cr} \quad (126)$$

$$\bar{N} = \frac{b}{a} \left[\varepsilon - \frac{\pi^2 w_0^2}{8a^2} - \frac{4S_{22}w_0}{\pi^2 R Z} \left(1 + \frac{b^2 S_{12}}{a^2 S_{11}} \right) \right] \quad (127)$$

where ε_{cr} can be calculated using equation (120). If the shell buckles in the narrow shell mode, it can be seen that the second equilibrium path is dominated by the membrane stiffnesses, whereas the bifurcation point is mainly controlled by the bending stiffnesses.

So far, a general predictive methodology for the compression strength of composite cylindrical shells has been developed through the energetic approach. On the basis of the present stability analysis, it can be expected that there will be an increasing trend to design composite compressive members in the postbuckling region, where the localized snap-through mode is prevented to fully utilize the material strength. From a practical standpoint, the impact resistance and damage tolerance analyses can be further integrated with each other so that composite designs can be tailored to maximize the overall performance, as highly impact resistant structures may not be very damage tolerant and vice versa.

VI. Experimental Verification

In this section, the predictive accuracy of the analytical model is demonstrated on the basis of a series of curved panel impact and CAI experiments. The experiments were designed with the primary aim to gain more insight into the impact induced damage development in cylindrical shells; therefore, the experiments are highly suitable for the verification of the analysis method with regard to impact resistance. As the panels have a strongly curved shape and possess a relatively large bending rigidity, the buckling mechanisms do not occur during the experiments; therefore, the results obtained are used to validate the damage tolerance solution involving the material failure mode. In Section V, the buckling stress of the localized snap-through mode has been shown to agree with the empirical formula, and the buckling and postbuckling solutions of the narrow shell mode have been theoretically verified on the basis of the existing solutions.

A. Experimental Procedure

The curved panels are manufactured from two thermoplastic composite materials. One is carbon fiber (T300) reinforced polyetherimide (PEI), consisting of 68% by volume of continuous fiber and 32% resin. The other is Aromatic Polymer Composite (APC-2), which is based on 62% by volume of carbon fiber (AS4) impregnated with a polyetheretherketone (PEEK) matrix. The T300/PEI and APC-2 prepregs are first compression molded to laminates in a Fontijne TP 1000 press using the manufacturer's recommended processing cycles. The laminates are subsequently thermoformed to the curved panels using a rubber molding technique under optimized conditions. The panels have a $[45_2, 0_2, -45_2, 90_2]_s$ quasi-isotropic lay-up, and their dimensions are specified in Figure 9.

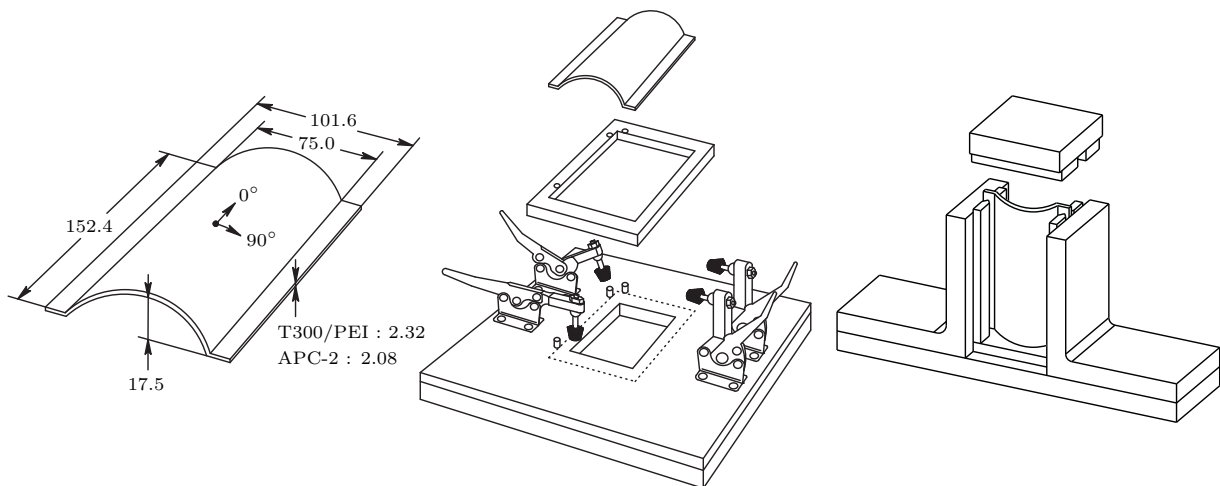


Figure 9. Dimensions of curved panel in mm, modified impact and CAI test fixture

The impact experiments are conducted on Dynatup 8250 drop weight impact machine, where the panels are mounted on the support fixture by way of a steel window frame. During the impact events, the panels are simply supported along the two rectilinear edges. The mass of the impactor is 3.035 kg, its diameter is 20 mm, and the nominal values of the impact energy are 2.5, 5, 10, 15 and 20 J. The damage area in the impacted panels is measured using a ultrasonic C-scanner. For the damage patterns, several impacted panels are cross-sectioned and examined under optical microscopes. The post-impact compression experiments are performed using a SCHENCK 250 kN tensile testing machine under a displacement controlled condition. The panels are simply supported between the knife edges along the vertical sides. The top and bottom edges of the panels are nominally clamped. For all tests, the compression speed is 0.1 mm/min. A detailed description of the experimental procedure including the design of the curved panels can be found in Huang²⁷.

B. Delamination Initiation

From the load deflection curves in Figure 10, it can be observed that the loading curves exhibit the same bi-linear form as in the previous flat plate experiments (see Huang et al.¹). The non-linear points, at which the loading curves start to depart from their initial linear parts, can be determined on the basis of the

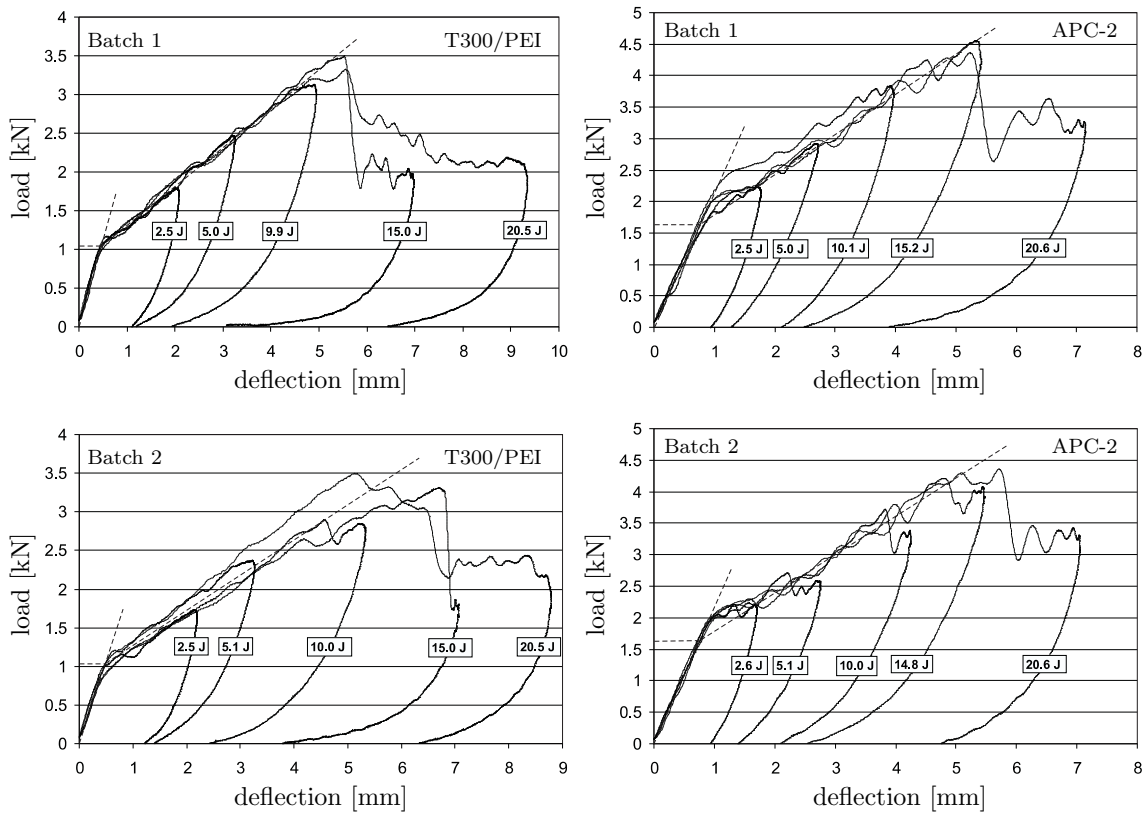


Figure 10. Experimental load deflection curves

intersection points of the best fit straight lines. In Table 1, an overview of the delamination threshold loads is presented, where the experimental values are basically the impact load levels at the non-linear points and the theoretical values are given by the flat plate model and the cylindrical shell model. Although there are small differences in the calculated maximum stresses and the damage states in the plies, the two models appear to give practically similar predictions for the delamination threshold loads. It can be established that the theoretical and experimental results are in good agreement with each other. Compared with the test values, the average values of the upper and lower bounds have provided an accuracy above 83.5%.

Table 1. Theoretical vs experimental delamination threshold loads

T300/PEI panels											
Model type	Condition of different layers			Lower bound	Upper bound	Average	Test value				
Plate model	45^\times	0^\times	-45^\surd	90_2^\times	-45^\times	0^\times	45^\times	0.84 kN	1.33 kN	1.08 kN	1.0 kN
Shell model	45^\times	0^\times	-45^\surd	90_2^\times	-45^\times	0^\times	45^\times	0.84 kN	1.33 kN	1.08 kN	
APC-2 panels											
Model type	Condition of different layers			Lower bound	Upper bound	Average	Test value				
Plate model	45^\times	0^\times	-45^\surd	90_2^\surd	-45^\times	0^\times	45^\times	1.03 kN	1.63 kN	1.33 kN	1.6 kN
Shell model	45^\times	0^\times	-45^\surd	90_2^\surd	-45^\surd	0^\times	45^\times	1.03 kN	1.64 kN	1.34 kN	

* \times : the layer contains transverse matrix cracks; \surd : the layer is undamaged.

C. Delamination Propagation

The results of the resultant fracture toughness calculations are summarized in Table 2, where n is the number of delaminations, Λ_{\min} is the local minimum of the objective function, λ_0 is the ellipticity ratio of the damage zone and G_c is the resultant critical energy release rate. For the T300/PEI panels, the global minimum of Λ_{\min} is first reached at 4 delaminations, and G_c becomes therefore equal to 3.7 kJ/m². For the APC-2 panels, the global minimum occurs at 6 delaminations, and this gives a G_c value of 7.0 kJ/m². In the previous study, the G_c values for the T300/PEI and APC-2 flat plates are found to be 2.6 and 3.0 kJ/m², respectively. The microscopic study confirms that the impacted curved panels indeed contain more delaminations compared with the corresponding flat plates. For the T300/PEI panels, the C-scan results show that the ellipticity ratio of the damage zones varies from 0.64 to 0.84. For the APC-2 panels, the ellipticity ratio varies from 0.52 to 0.84, when the panels of 2.5 and 2.6 J are excluded (In these two case, the damage zones are relatively small and approximately circular.). This means that the linear near field analysis predicts reasonably well the ellipticity ratios of the damage zones.

The theoretical and experimental slopes of the delamination propagation curves are listed in Table 3, showing that the actual slopes are amply overestimated by the flat plate model, and they are more accurately predicted by the cylindrical shell model. In Figure 11, the damage area S is plotted against the peak impact load P_{max} and the impact energy E . In the results from the flat plate model, it is a pure coincidence that the T300/PEI energy graph and the APC-2 load graph correlate with the measurements, as the errors in the parameters such as G_C and Υ can compensate for each other. As expected, the T300/PEI load graph and the APC-2 energy graph deviate significantly from the measurements. Among the results from the cylindrical shell model, the following theoretical graphs are found to be in satisfactory agreement with the experimental data: the T300/PEI energy graph, the APC-2 load graph and the APC-2 energy graph. It can be seen that these calculated curves go right through the middle of the measured data points that have a certain scattering. In the worst case of the T300/PEI load graph, a sizeable improvement in the predictive accuracy has been achieved compared with the plate model. That the calculated values in this particular case are slightly lower than the measured values can be explained by the occurrence of small-scale fiber breakage in the 0° plies, as the fiber tensile strength of T300 carbon fiber is relatively low. For illustrative purposes, the dotted curve is added, which can be produced by decreasing the longitudinal stiffness of the 0° plies. In brief, the current model is capable of providing adequate predictions of the process of impact induced damage development in cylindrical composite structures, whereas the previous model may only serve as a rapid tool for the determination of the delamination threshold load.

Table 2. Determination resultant critical energy release rate

n	T300/PEI			APC-2			Location delaminations
	Λ_{min}	λ_0	G_C	Λ_{min}	λ_0	G_C	Sublaminaes
1	0.029	0.642	1.6 kJ/m ²	0.048	0.704	1.8 kJ/m ²	[45,0,-45],[90 ₂ ,-45,0,45]
2	0.015	0.639	1.6 kJ/m ²	0.018	0.645	1.9 kJ/m ²	[45,0,-45],[90 ₂],[-45,0,45]
3	0.014	0.635	2.7 kJ/m ²	0.016	0.631	3.1 kJ/m ²	[45,0,-45],[90 ₂],[-45],[0,45]
4	0.011	0.618	3.7 kJ/m ²	0.013	0.614	4.2 kJ/m ²	[45,0],[-45],[90 ₂],[-45],[0,45]
5	0.011	0.608	4.4 kJ/m ²	0.013	0.605	6.1 kJ/m ²	[45,0],[-45],[90 ₂],[-45],[0],[45]
6	0.011	0.597	6.1 kJ/m ²	0.012	0.594	7.0 kJ/m ²	[45],[0],[-45],[90 ₂],[-45],[0],[45]

Table 3. Slopes of delamination propagation curves

Specimens	Experimental	Plate model	Shell model
T300/PEI	0.50 kN/mm	1.05 kN/mm	0.61 kN/mm
APC-2	0.61 kN/mm	0.94 kN/mm	0.67 kN/mm

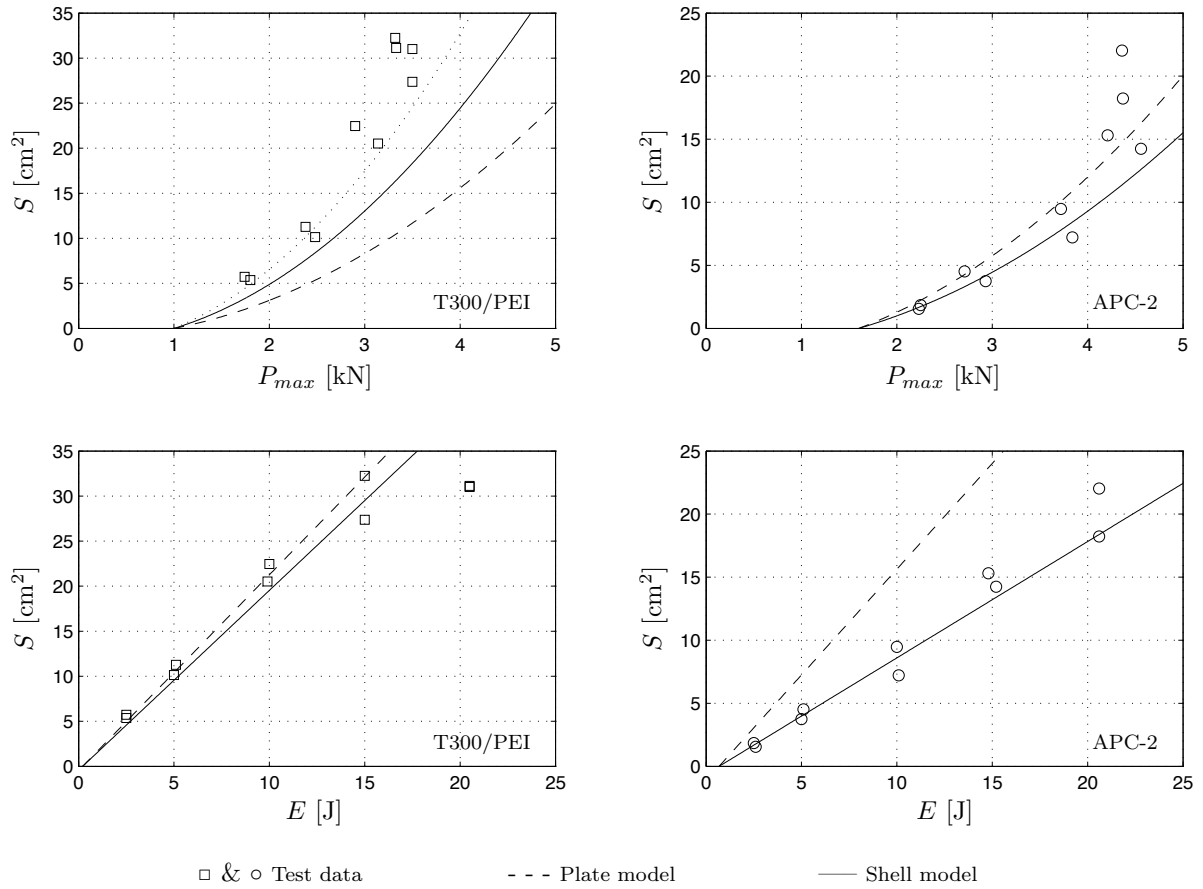


Figure 11. Damage area as function of peak impact load and impact energy

D. Post-impact Compression

As expected, the non-impacted panels fail at the top edge, and the measured failure stress σ'_m is slightly lower than the actual laminate strength σ_m because of local imperfections. The impacted panels fail through the middle where the damage zone is located, and the damage has mainly extended in the direction perpendicular to the compression direction. In Figure 12, the residual compression strength is plotted against the damage zone width, one as a percentage of the measured undamaged strength and the other as a percentage of the total panel width. It turns out that the data points can be scaled onto a single linear master curve. The short plateau in the beginning can be explained by the fact that σ'_m is used as the reference strength instead of σ_m . The experimental results support the theoretical predictions that the panels fail due to the material compression failure mode and the residual compression strength varies linearly with the damage zone width. In point of fact, the CAI tests of flat plates using an anti-buckling guide yields similar results as the current tests, as there occurs the same failure mechanism in the two situations.

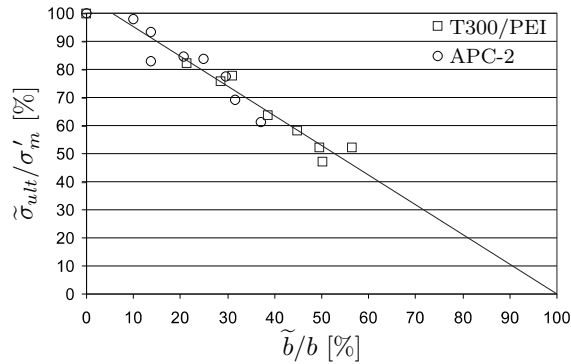


Figure 12. Residual strength vs normalized damage width

VII. Conclusions

In the present study, a physically well-founded model has been developed for the impact resistance and damage tolerance characteristics of cylindrical composite shells. The general conclusions are as follows:

1. For thin elastic shells, Love's theory is general, parsimonious and accurate. The theory is consistent with the 3D elasticity theory, the 2D plate theory and the 1D beam theory, and can be reconciled with other existing shell theories with varying degrees of complexity. As a baseline theory, Love's theory can be extended to account for the material anisotropy and geometrical non-linearity. If the wavelength of the deformations is limited, Love's theory can be further reduced to Donnell's theory, which can still find a wide range of applications in the engineering practice. It appears that the use of the Airy stress function is a convenient and effective way to calculate the membrane deformations and stresses.
2. The large deflection analysis reveals that the snap-through buckling is a manifestation of a strong geometrical non-linearity, whereby the membrane deformations contain an inherent instability that is connected with the convexity concavity transition of the shell surface.
3. With regard to the impact resistance, various analytical solutions that were derived for flat plates remain applicable for cylindrical shells, if the following parameters are adapted: the damage state due to matrix cracking, the ellipticity of the damage zone, the resultant critical energy release rate and the membrane stiffness of the damage zone. Compared with a flat plate, the curvature of a shell leads to quantitative rather than qualitative changes in the process of impact induced damage development.

4. The buckling behavior of thin cylindrical shells is characterized by comparatively short waves in both the longitudinal and circumferential directions. When the shell curvature increases, a transition occurs from the narrow shell mode to the localized snap-through mode. The energy balance equation that applies to the bifurcation point remains valid for the entire postbuckling path. The derivation of the buckling and postbuckling solutions through the energy method is appreciably more expeditious than by solving the governing equilibrium equations.
5. The analytical model proposed is expected to be beneficial to bridge the gap that frequently exists between the material database and the full-scale component response in the field of aerospace design. It is self-evident that composite shell structures exhibit considerably more complex failure behavior compared with their metallic counterparts. The point illustrated here is the fact that the strength characteristics of composite shell structures remain excellently analyzable, thereby enabling highly efficient designs to be realized that are safe against multiple failure mechanisms.

Acknowledgments

The analytical work was carried out at Crea Mech Co., Ltd in the period from 2006 to 2011. The experimental work was performed at University of Twente under the BRITE/EURAM III Project, Adaptive Composite Delamination Modeling, BE-3580. The author would like to thank A. de Boer, R. Akkerman and F. Eising from University of Twente for their constructive feedback and stimulating discussions. The author also expresses his gratitude to the reviewers for their helpful comments and suggestions.

References

- ¹Huang, K. Y., de Boer, A., and Akkerman, R., "Analytical modeling of impact resistance and damage tolerance of laminated composite plates," *AIAA Journal*, Vol. 46, No. 11, 2008, pp. 2760–2772.
- ²Raymer, D. P., *Aircraft design: A conceptual approach*, AIAA Inc., Reston, Virginia, 1999.
- ³Ambur, D. R. and Starnes Jr., J. H., "Effect of curvature on the impact damage characteristics and residual strength of composite plates," *39th AIAA/ASME/ASCE/AHS/ASC Structures, Structural Dynamics, and Materials Conference*, California, 1998, pp. 1556–1567.
- ⁴Wardle, B. L. and Lagace, P. A., "Importance of instability in impact response and damage resistance of composite shells," *AIAA Journal*, Vol. 35, No. 2, 1997, pp. 389–396.
- ⁵Flügge, W., *Statik und Dynamik der Schalen*, Springer, Berlin, 1934.
- ⁶Koiter, W. T., "On the nonlinear theory of thin elastic shells," *Proceedings of the Koninklijke Nederlandse Akademie van Wetenschappen*, Vol. 69 of Series B, Amsterdam, 1966, pp. 1–54.
- ⁷Sanders Jr., J. L., "Nonlinear theories for thin shells," *Quarterly of Applied Mathematics*, Vol. 21, No. 1, 1963, pp. 21–36.
- ⁸Love, A. E. H., *A treatise on the mathematical theory of elasticity*, Cambridge University Press, Cambridge, 1927.

- ⁹Morley, L. S. D., “An improvement on Donnell’s approximation for thin-walled circular cylinders,” *Quarterly Journal of Mechanics and Applied Mathematics*, Vol. 12, No. 1, 1959, pp. 89–99.
- ¹⁰Simmonds, J. G., “A set of simple, accurate equations for circular cylindrical elastic shells,” *International Journal of Solids and Structures*, Vol. 2, 1966, pp. 525–541.
- ¹¹Donnell, L. H., *Beams, plates and shells*, McGraw-Hill, New York, 1976.
- ¹²Lord Rayleigh, J. W. S., “On the infinitesimal bending of surfaces of revolution,” *Proceedings of the London Mathematical Society*, Vol. 13, 1881, pp. 4–16.
- ¹³Leissa, A. W., *Vibration of shells*, Scientific and Technical Information Office, NASA, Washington, DC, 1973.
- ¹⁴Kirchhoff, G. R., “Über das Gleichgewicht und die Bewegung einer elastischen Scheibe,” *Journal für die reine und angewandte Mathematik*, Vol. 40, 1850, pp. 51–88.
- ¹⁵Riks, E., “An incremental approach to the solution of snapping and buckling problems,” *International Journal of Solids and Structures*, Vol. 15, 1979, pp. 524–551.
- ¹⁶Ventsel, E. and Krauthammer, T., *Thin plates and shells - Theory, analysis, and applications*, Marcel Dekker, New York, 2001.
- ¹⁷Lorenz, R., “Achsensymmetrische Verzerrungen in dünnwandigen Hohlzylindern,” *Zeitschrift des Vereines Deutscher Ingenieure*, Vol. 52, No. 43, 1908, pp. 1706–1713.
- ¹⁸Timoshenko, S. P. and Gere, J. M., *Theory of elastic stability*, McGraw-Hill, New York, 1936.
- ¹⁹Koiter, W. T., *The stability of elastic equilibrium*, Ph.D. thesis, University of Delft, Delft, The Netherlands, 1945.
- ²⁰Jones, R. M., *Mechanics of composite materials*, Taylor & Francis, Philadelphia, 1998.
- ²¹von Kármán, T., “Festigkeitsprobleme im Maschinenbau,” *Encyclopädie der Mathematischen Wissenschaften*, Vol. IV/4, 1910, pp. 311–385.
- ²²Timoshenko, S. and Woinowsky-Krieger, S., *Theory of plates and shells*, McGraw-Hill, New York, 1959.
- ²³Huang, K. Y., “Energy based strength analysis of fiber reinforced polymer composites,” International SAMPE Conference and Exhibition, Beijing, China, 6-8 May, 2019.
- ²⁴Lukasiewicz, S., *Local loads in plates and shells*, Sijthoff and Noordhoff, Alphen aan den Rijn, the Netherlands, 1979.
- ²⁵Timoshenko, S. and Goodier, J. N., *Theory of elasticity*, McGraw-Hill, New York, 1951.
- ²⁶Matthews, F. L., Davies, G. A. O., Hitchings, D., and Soutis, C., *Finite element modelling of composite materials and structures*, CRC Press, Boca Raton, 2000.
- ²⁷Huang, K. Y., *On impact induced delamination and residual compression strength of composite structures*, Ph.D. thesis, University of Twente, Enschede, The Netherlands, 2001.